PERMEABILITY OF HYBRID COMPOSITES SUBJECTED TO EXTREME THERMAL CYCLING AND LOW-VELOCITY IMPACTS

A Thesis
Presented to
The Academic Faculty

By

Amelia Ann Case

In Partial Fulfillment
Of the Requirements for the Degree
Master of Science in Mechanical Engineering

Georgia Institute of Technology

November 2004

PERMEABILITY OF HYBRID COMPOSITES SUBJECTED TO EXTREME THERMAL CYCLING AND LOW-VELOCITY IMPACTS

Approved by:

Dr. W. Steven Johnson, Chairman

Dr. David L. McDowell

Dr. Erian A. Armanios

Date Approved: 11/19/2004

ACKNOWLEDGEMENTS

First and foremost I would like to thank my fiancé, Scott, and my parents, Libby and Les, for all of their help and support. Without the support of my parents, fiancé, family-to-be, long time friends, and my more recent grad school friends, I don't think this would have been possible. Thanks for chilling me out when things got stressful and for being excited along with me when things were going great.

I would also like to thank my advisor, Dr. Johnson, for giving me the opportunity to work on such an great research project, and also for all of his advice and suggestions along the way, without which this project could have never happened. I would also like to mention and thank my thesis committee members, Dr. Erian Armanios and Dr. David McDowell. I would like to thank the Composites Research Center at Georgia Tech, for the use of their equipment and facilities, and Dr. Caihua Cao for spending the time to teach me how to lay-up my specimens and use the autoclave.

The help of Rick Brown and Robert Cooper, MPRL's laboratory technicians, was invaluable to getting this research completed smoothly and on time. I would especially like to thank Rick for all of his help with setting up and maintaining the testing equipment used for this project, and I would like to thank Robert for all of his help troubleshooting the impact test equipment. I would like to thank Ed Li, from Boeing, and Brian Jensen, from NASA LaRC, for providing research samples of β-Titanium, and Dr. Ravi Deo, from Northrop Grumman, for sending the IM7/977-2 prepreg material.

And finally, I would like to thank the fellow members of Team Johnson and the friends I have met while in graduate school, especially Matt, Don, Kyle, Carrell, Amar,

Shelby, Crystal, and Connor. Thanks for all of your help and input on this project and also for livening up the long hours of studying with all of the jokes and political debates.

TABLE OF CONTENTS

LIST OF TABLES

LIST OF FIGURES

LIST OF SYMBOLS AND ABBREVIATIONS

8250	Dynatup 8250 impact test machine
$[X/Y]_{ns}$	Symbol for symmetric lay-up of composite
“	inch, unit of length
‘	foot, unit of length
@	at
α, CTE	coefficient of thermal expansion
$	Dollars
o	degree symbol
^{o}C	degree Celsius, unit of temperature
^{o}F	degree Fahrenheit, unit of temperature
ASTM	American Society for Testing and Materials
CAD	computer aided design
CFRP	carbon fiber reinforced plastics
CIE	critical impact energy
cm	centimeter, unit of length
DC-XA	Delta Clipper Advanced, prototype RLV
ε	strain
E_a	absorbed energy
EB	electron beam cured composite
EX 1552	epoxy matrix made by Bryte Technologies
ft	feet, unit of length

ft-lb	foot-pounds, unit of energy
g	gravity, 9.81 m/s or 32.2 ft/s
GRC	NASA GRC
GPa	giga-Pascal, unit of strength
HM	high modulus carbon fiber
HS	high strength carbon fiber
IE	impact energy
IM7	carbon fiber made by Hexcel
in	inch, unit of length
in/sec-psi	inch per second-pound per square inch, unit of rate
of	permeation
J	Joule, unit of energy
K	Kelvin, unit of temperature (0K = -273 ^{o}C)
kPa	kilo-Pascal, unit of pressure
ksi	kips per square inch, unit of strength
lb	pound, unit of force
LH_2	liquid hydrogen
LHe_2	liquid helium
LN_2	liquid nitrogen
LO_2	liquid oxygen
m	meter, unit of length
m/s	meters per second, unit of velocity
min	minute

MPa	mega-Pascal, unit of pressure (106 Pa)
N	Newton, unit of force
NASA	National Aeronautics and Space Administration
NASA GRC	NASA Glenn Research Center
NASA LaRC	NASA Langley Research Center
NASA MSFC	NASA Marshall Space Flight Center
NGLV	next generation launch vehicle
nm	nanometer, unit of length
Pa	Pascal, unit of pressure
PETI-5	Thermoplastic matrix material made by Cytec
PMC	polymer matrix composite
psi	pounds per square inch, unit of pressure or strength
RLV	reusable launch vehicle
SBS	short beam shear
SCC/sec-in2	standard cubic centimeter per second-inch squared, unit of permeability
SLI	space launch initiative
SSTO	single state to orbit
σ	stress
Tg	glass transition temperature
TPS	thermal protection systems
V	velocity at impact
V_f	fiber volume fraction

V_r	rebound velocity
v	Poisson's ratio
W_{flag}	width between leading edges on the velocity flag of the Dynatup 8250
X-33	prototype RLV

SUMMARY

The current cost to transport payload into orbit is $10,000 per pound, so NASA would like to reduce overall vehicle weight, which will in turn reduce the cost per pound of payload for their next generations of reusable launch vehicles (RLVs). Composite materials are ideal candidates for aerospace applications due to their high strength-to-weight ratios and their excellent fatigue resistance. By switching out the current aluminum LH_2 and LO_2 cryogenic fuel tanks for composite fuel tanks on the next generations of reusable launch vehicles (RLVs), a 40% reduction in tank weight can be achieved. This reduction in tank weight translates to a 14% reduction in overall vehicle weight.

One of the main issues surrounding using composite materials for this extreme application, or any material for that matter, is that permeation of the cryogenic fuel can cause a catastrophic failure. Small concentrations of hydrogen of 4% in air are flammable, and higher concentrations can be explosive. These cryotanks are exposed to extreme thermal stresses as well as low-velocity impacts, both of which can cause damage within the composite and thereby lead to fuel permeation.

NASA is very concerned that the cryotanks and fuel lines will be exposed to low-velocity impact events during installation and maintenance. These impact events could be caused by dropped tools or inadvertent bumping. Impacts with enough energy can cause various modes of damage within the composite, which can possibly lead to fuel permeation. Previous research determined that impacts which didn't leave any visible

damage could still cause the composites to leak. Additionally, some of the sample feedlines have been found to leak before any impact events whatsoever.

Another concern is that these cryotanks are subjected to extreme changes in temperature due to the cryogenic temperature of the fuel and the elevated temperatures of the vehicle upon re-entry into the atmosphere. Due to the mismatch in coefficient of thermal expansion (CTE) between the fibers and the matrix, changes in temperature cause stresses to develop within the composite. When the temperature changes are extreme enough, these thermal stresses can cause matrix microcracking which can lead to fuel permeation.

Previous research on the effectiveness of surface coatings for improving impact resistance and thermal resistance found that the coatings were able to significantly increase the amount of impact the composites could withstand before leaking. Unfortunately all of the coatings failed to a greater or lesser degree during the thermal cycling. Thereby rendering these coated composites unacceptable materials for use on the cryogenic fuel tanks and feedlines. Results from this research led to the idea of introducing a ductile, thermally compatible layer within the composite in an attempt to improve its resistance to damage due to impact and thermally induces stresses which can lead to fuel permeation. The purpose of embedding the barrier, or interleaf, within the composite, as opposed to on the surface, was to avoid the thermal shock experienced by the coatings.

The purpose of this research is to develop a method for making polymer matrix composite (PMC) materials more robust for the application of extreme temperatures and impact stresses. Specifically, this research attempts to determine if a “barrier” layer,

embedded during manufacture, can reduce a PMC's permeability after thermal cycling and low velocity impact events. Upon thermal cycling and impacting these hybrid composites, damage is still expected to occur in the composite material, but in theory, the barrier layer would be sufficiently ductile to remain intact even when the composite cracked, thereby assisting the composite in retaining its impermeability.

The baseline composite material for this research was a graphite/epoxy (IM7/977-2) toughened epoxy system with a $[0/90]_{2S}$ lay-up. Barrier layer candidates included two thicknesses of aluminized Mylar®, two thicknesses of aluminum foil, and two β-Ti 15-3 films, one coated with resin and one without. Barrier layer candidates were evaluated to determine thermal compatibility with the graphite/epoxy composite. Control composites as well as hybrid composites containing the proposed barrier layers were manufactured in-house using an autoclave. All specimens were leak tested with pressurized Helium, using equipment based on an apparatus used in previous experiments at NASA. Thermal cycling was performed on the control and hybrid composites to simulate the extreme temperatures that the composite cryotanks would be exposed to during a typical flight cycle. The control and hybrid composites were subjected to thermal cycling to determine if the barrier layers could reduce the composite's permeability after extreme thermal cycling.

Drop-weight impact tests were performed using a Dynatup 8250 test machine, to simulate impacts due to inadvertent bumping and/or dropped tools during installation and maintenance. Using the drop-weight impact tests and the leak testing apparatus, the critical impact energy (CIE) for each type of hybrid and the control

composites was determined. The CIE is defined as the most amount of impact energy the composite can withstand while remaining impermeable.

Control composites as well as hybrid composites containing the candidate barrier layers were successfully manufactured using an autoclave in the Composites Processing Lab, belonging to the Aerospace Engineering department at Georgia Tech. All specimens were found to be leak free after fabrication. Thermal cycling did not cause leaks or delaminations in any of the control or hybrid specimens, although slight delamination was observed in the corners of the β-Ti 15-3 (no resin) and Mylar® hybrids after holes were drilled in the corners. The β-Ti 15-3 (with resin) outperformed all other hybrids, exhibiting an increase in critical impact energy of more than 3.5 times that of the control. The Mylar® hybrids performed next best under impact, with an improvement factor of approximately 2.8 times the control, while the Aluminum foil hybrid specimens exhibiting a CIE of approximately 1.8 times that of the control.

The purpose of this research was to develop a method for making graphite/epoxy composites more resistant to thermal stresses and low-velocity impacts by embedding a durable barrier layer material as the middle ply within the composite. Once PMCs can be toughened to resist damage caused by extreme temperatures and impacts they become viable options for cryogenic fuel tank and feedline material for NASA's next generation RLVs. The results of this research suggest that the addition of an embedded barrier layer can increase a graphite/epoxy composite's resistance to thermal stresses and low-velocity impacts, by allowing the composites to remain leak free after thermal cycling and increasing the amount of impact the composite can withstand before leaking, thereby making the use of hybrid composites extremely promising for applications of extreme temperatures and stresses.

CHAPTER 1 INTRODUCTION AND RESEARCH OBJECTIVES

Composites are currently used in a variety of applications, from aircraft fuselages and engine components, to tennis racquets and golf clubs. Due to their high strength-to-weight ratios and excellent fatigue resistance, composites are particularly ideal candidates for aerospace applications, where vehicle weight and fatigue behavior are critical design factors. Although the use of composites has many advantages, these complex materials present new issues surrounding their mechanical behavior. There exists a widespread need for composite materials that can withstand extreme changes in temperature and low-velocity impacts while remaining leak free. One such application where these properties are critical, is with the cryogenic LH_2 and LO_2 fuel tanks and feedlines of NASA's next generation reusable launch vehicles (RLVs). NASA would like to reduce the cost per pound of payload down from the current \$10,000/lb to \$1000/lb for the 2nd generation RLV, and finally down to \$100/lb for the 3rd generation RLV. Using composite materials for the cryotanks, as opposed to aluminum used previously, translates to an overall reduction in vehicle weight of 14%.[1]

The major concern with using composite materials for this application is that these structures will be exposed to extreme changes in temperature and low-velocity impacts which can lead to fuel permeation. Permeation of the cryogenic fuel can lead to a catastrophic failure, thus virtually any leakage is unacceptable, and so it is this property that is of primary concern for this research. The purpose of this research is to develop durable hybrid graphite/epoxy composites capable of withstanding extreme temperatures and impacts while remaining impermeable.

Specifically, this research will attempt to determine if the addition of an embedded barrier layer within a graphite/epoxy composite will:

- allow a higher percent of composite structures to be leak-free after fabrication
- allow a higher percent of composite structures to remain impermeable after extreme thermal cycling
- allow the composite structures to withstand greater impacts while remaining impermeable (i.e. increase their critical impact energy)

The expectation is that, through embedding a barrier layer within the laminate, the resistance of the graphite/epoxy composite to thermal stresses and impacts will be improved. In theory, damage would still occur in the graphite/epoxy composite, but the barrier layer would be sufficiently ductile to remain intact, thereby allowing the laminate to retain its impermeability.

The results of this research are divided into the following chapters. Chapter 2 discusses RLV technology, thermal cycling, impacts and permeability of composites, as well as previous research on coated and hybrid composites. Chapter 3 describes specifics of the materials used in this research; composite constituents and barrier layer materials. Chapter 4 discusses the experimental procedure and details of the equipment used in this research. Chapter 5 outlines the results obtained from the manufacture of specimens, leak testing, thermal cycling and impact testing. Final conclusions and trends are mentioned in Chapter 6, and the lessons learned and recommendations for future work are discussed in Chapter 7.

CHAPTER 2 BACKGROUND AND LITERATURE REVIEW

In order for composites to become a viable option for applications of extreme temperatures and stresses, they must be toughened to resist the damage caused by thermally induced stresses and impacts. The objective of this research is to develop durable hybrid polymer matrix composites that are capable of withstanding extreme thermal cycling and low-velocity impacts while retaining their impermeability. But before this can be accomplished, the issues surrounding the mechanisms by which impacts and thermal stresses effect permeability must be understood. This chapter will begin with a discussion of reusable launch vehicle (RLV) technology and the motivation behind this research, discuss research conducted in the areas of thermal cycling, permeability and impact mechanics, and then finish with a discussion of previous research on coated laminates and hybrid, or interleaved, composites.

2.1 RLV Technology

This section will describe previous research conducted on composites for use on the next generations of NASA's reusable launch vehicles, as well as two projects that attempted using composite fuel tanks, the DC-XA and the X-33. As discussed previously, due to their high strength-to-weight ratios, composites are ideal candidates for applications where weight is of particular concern. One such application is with NASA's next generations of reusable launch vehicles (RLVs). It currently costs $10,000 per pound to send payload into orbit[1], so NASA would like to reduce vehicle weight so that

more payload can be carried into space, thereby reducing the cost per pound of payload[2]. Previously, NASA had plans for a second generation RLV set to be produced in 2010 and a third generation RLV, set to be produced in 2025.[1] The cost per pound of payload was set to be reduced to $1000, for the second generation RLV, and further down to $100, for the third generation RLV second generation RLV. Since then, NASA has a redirect[3] from an all-cryogenic next-generation reusable space launch vehicle toward a smaller vehicle that uses hydrocarbon fuel in its first stage and liquid hydrogen in its second, and combined these two initiatives and named it the Next Generation Launch Vehicle (NGLV). This research pertains to the previous plans for the LH_2 and LO_2 fuel tanks and feedlines on the 2nd generation RLV.

NASA determined in 1993 that changing out the Aluminum cryogenic fuel tanks for composites cryotanks could reduce the weight of the tank by 40%, which translates into an overall vehicle weight savings of 14%.[1] Many metal feedline designs are driven by the need for the line to withstand its own weight rather than sustain the pressures of the fuel, and since composites have such high strength-to-weight ratios, they do not have this problem[4].

Under the Space Launch Initiative (SLI), research has been conducted surrounding the use of composite materials for the fuel tanks and fuel lines for both the X-33 concept RLV and the Delta Clipper (DC-XA). These single state to orbit (SSTO) RLVs would have the ability to take-off like a traditional airplane, travel into space, then return to land on Earth. The 2nd and 3rd generation RLVs were intended to be similar to the X-33, using polymer matrix composites as structural components in cryogenic fuel tanks. Up until these vehicles, no one had attempted to make cryogenic tanks out of composite materials, therefore, the viability of this application of composites was a major

concern. Northrop Grumman reported on the investigation of two different cryotank designs, the skin-stringer and the sandwich structure design[5]. The design chosen for the DC-XA was a skin-stringer design[6] and the design chosen for the X-33 was a sandwich structure[7].

The DC-XA was an adaptation of a McDonnell-Douglas vehicle that had previously used metal tanks. This vehicle contained composite LH_2 and LO_2 fuel tanks as well as composite feedlines. The feedline design consisted of several fundamental requirements[8]:

- Acceptable hydrogen permeability levels for flight hardware
- Composite-to-composite adhesive joints
- Composite-to-metallic adhesive joints
- Composite-to-composite flange interface
- Composite elbows (90° bends in tubes)
- Composite valves for LH_2

These feedlines consisted of IM7/8552 eight harness weave prepregs with a [0/90/±45/±45/90/0] lay-up. A sample of a LH_2 feedline is depicted in Figure 2.1.1 below.

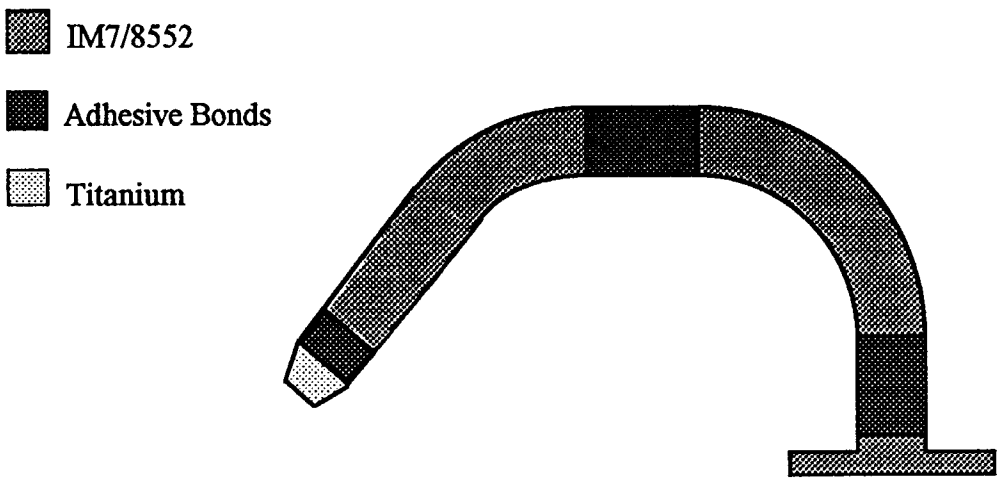

Figure 2.1.1 Sample LH_2 Composite Feedline[8]

Dr. Nettles[8] tested the permeability of sample feedlines as well as flat panel specimens to pressurized Nitrogen gas. He also tested composites bonded to titanium washers to determine the permeability to the bondlines. His experiments yielded panel permeabilities on the order of 10^{-6} in^3/sec-psi and bondline permeabilities ranging from $5x10^{-6}$ to $6x10^{-3}$ in^3/sec-psi. Nettles then subjected specimens to thermal cycles from LN_2 (-196°C) to elevated temperatures (100°C) on the specimens and found a very small change in permeability.

Since the possibility of an accidental low-velocity impact event was of concern, he also conducted drop-weight impact tests to simulate a dropped tool or inadvertent bump during installation or maintenance. Nettles performed impacts with a variety of different impacting tips to determine the damage mechanisms caused by different types of impact. He used a sharpened bolt tip, a hemispherical tip and a blunt tip.

He determined that, with a hemispherical tip or a blunt tip, matrix damage was the dominating damage mechanism involved. He also observed that the visible damage on

the surface could not reliably determine the rate of permeability. He found that impacts as low as 0.79 ft-lb would cause permeation in all cases[9]. The specimens impacted with a sharpened bolt tended to have complete punctures, but that when the impact did not cause complete penetration of the composite there was not always sufficient matrix cracking for permeation to occur. Through conversations between Dr. Nettles and Ben Findley[10], it was determined that another issue with these feedlines was that many were found to be permeable prior to any impact events whatsoever. It was determined that proper material processing was crucial to obtaining a leak free feedline.

The first of several test flights of the DC-XA took place on May 20, 1996[11]. During this first flight, lasting one minute, the vehicle reached a maximum altitude of 800 ft. Using composite materials for the fuel tanks on the DC-XA translated to a 1200 lb weight savings from the weight of previously used metal tanks. Unfortunately, at the end of the fourth test flight, the landing gear failed to deploy and the tanks were destroyed when the vehicle collapsed.

The X-33 concept RLV was the precursor to the 2nd generation RLV, using composites for cryogenic fuel tanks. These tank walls were constructed of polymer matrix composite laminates bonded to a honeycomb core. Figure 2.1.2 displays a schematic of the X-33 concept RLV.

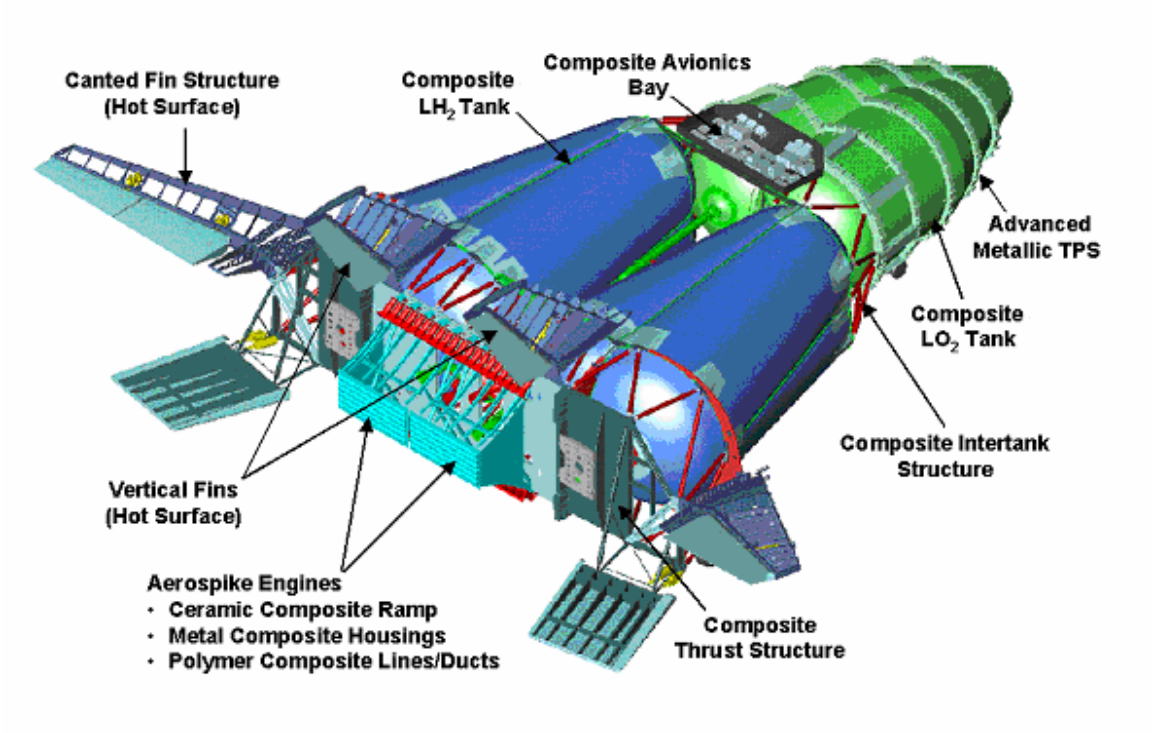

Figure 2.1.2 X-33 Concept RLV[2]

Charles Gudatis[12], from Lockheed Martin, conducted qualification testing of high pressure composite cryotanks. These tanks were made of filament wound graphite/epoxy with a titanium lining, and were designed to withstand a service pressure of 3200 psi and were tested with pressures up to 6400 psi. The tanks were found to remain impermeable with 6400 psi LH_2. Gudatis also found negligible degradation occurred after the pressure was held for four hours and bled off quickly to simulate take off and the temperature elevated to simulate landing. The sandwich structures for the two LH_2 tanks were subjected to preflight proof tests. During these proof tests the tank failed when, due to fuel permeation through the interior face sheet composite, the pressure increased in the core of the sandwich tank causing the face-sheets to debond and separate from the core material[13].

Previous attempts to utilize composite materials for use on fuel tanks and feedlines for cryogenic space applications have solidified the need to improve these materials. The research described in this thesis attempts to toughen these materials so they can be considered viable options for these applications of extreme temperatures and stresses.

2.2 Thermal Loading and Permeability

One issue surrounding the use of composites on the RLVs cryotanks and feedlines is that these structures are exposed to extreme changes in temperatures. Extreme thermal cycling can damage the composite and lead to fuel permeation. This section will describe the temperatures experienced by the cryotanks of the RLVs and the damage mechanisms by which extreme changes in temperature can cause fuel permeation through composite cryotanks.

The pre-flight temperature of the empty cryotanks is controlled by the ambient temperature of the surrounding environment, approximately 27°C (80°F). Upon fueling, the temperature of the tanks rapidly drops to the temperature of the cryogenic fuel. The LO_2 tanks will be subjected to temperatures as low as -183°C (-298°F), while the LH_2 tanks will be subjected to temperatures as low as -253°C (-423°F).[2] Not only must the cryotanks withstand these extremely cold temperatures, they must also withstand elevated temperatures upon re-entry into the Earth's atmosphere. The outer surface of the RLV will be exposed to extremely high temperatures directly, but the cryotanks will be shielded from a large percent of this heat, due to the insulation and thermal protection

systems (TPS). The cryotanks themselves will be exposed to elevated temperatures of approximately 126°C (260°F). This thermal cycle represents a change in temperature of 380°C (680°F). The Figure 2.2.1 shows a typical flight cycle that the composite cryotanks must endure.[2]

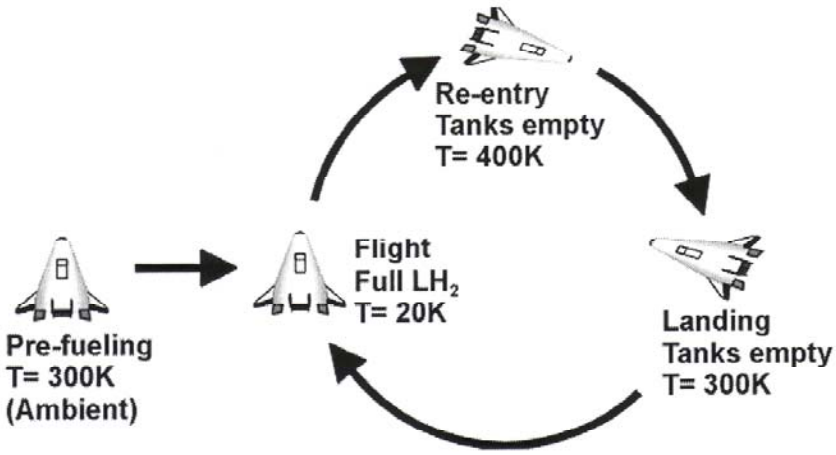

Figure 2.2.1 Typical RLV Cryotank Temperature Cycle[2]

This large change in temperature can lead to degradation of the material and the structure as a whole. The large changes in temperature can cause matrix microcracking or debonding between the joints which can lead to fuel permeation. Thermal mismatch, particularly in adhesive bonding scenarios, can cause structural failure. For purposes of this research, thermal loads that lead to fuel permeation will be of primary concern.

It has been found that carbon/epoxy composites are very vulnerable to microcracking caused by thermal cycling.[2] Due to the mismatch of CTE between the fibers and the matrix, this change in temperature causes stresses to build up between the fiber and matrix and also between the plies of different fiber orientation. With PMCs, the

matrix generally has a much larger CTE than the fiber. This means, for example, that as the temperature drops, the matrix wants to contract much further than the fibers want to contract, which induces stresses in the matrix and fiber, as well as in the interface between the two materials. Also, due to the difference in fiber orientation between plies of a laminate, the plies have a different CTE in the principal directions. This is the reason for the development of thermal stresses between plies upon a change in temperature.

Whitley and Gates[14] studied five different lay-ups of IM7/PETI-5 and found that cracking is influenced by the composite's lay-up. Additional research has been conducted to model composite lay-up effects on thermal stresses and matrix cracking. Thermal loads can cause cracks to develop in the matrix material perpendicular to the fibers as well as in the fiber-matrix interface. These studies found the cracking first occurs in the matrix of the 90° plies and then progress into the 0° plies. The 90° plies were found to have twice the crack density of the 0° plies, which can be attributed to the lower strength and stiffness of the 90° plies, dominated by matrix properties in the direction of loading[15, 16].

McManus *et al* [17] conducted studies on graphite/epoxy composites and found that these composites can crack due to the thermally induced loads caused by the RLV flight cycle and this microcracking reaches a fairly constant density after just a few cycles. Cracking in the matrix material was found to initiate after only a few cycles between -213°C (60K) and 127°C (400K). The maximum microcracking density generally was reached after 5 cycles.[17] This microcracking was found to be strongly related to the permeability of the composite.

Since composites have been found to be susceptible to cracking due to thermal cycling which can lead to permeation, this presents a complicated problem for applications of composite materials as cryogenic fuel tanks. Ben Findley[10] noted in his Master's thesis that permeation of fuel can cause a catastrophic failure because concentrations of hydrogen of 4% in air are flammable, and concentrations of 18.3 % or higher are explosive. Permeability guidelines for the National Aerospace Plane project required permeation rates between 10^{-4} and 10^{-3} SCC/sec-in^2 (standard cubic centimeter per second per square inch).

Kumazawa *et* al[18] found that cracks in the matrix material not only reduce the mechanical performance of the composite, but also led to paths large enough for gaseous helium to permeate through. It has been found that laminates with more variation in the ply orientation have greater permeations than laminates with fewer ply orientations. This is because, in the case of a laminate with many ply orientations, the cracks had a better chance to overlap, therefore creating a complete leak path through the thickness of the composite. Figure 2.2.2 displays an example of how cracks in plies of different orientation can link up and cause fuel permeation.

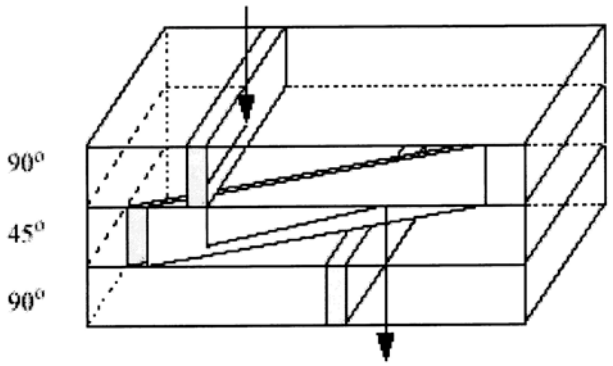

Figure 2.2.2 Cracks Link Up to Allow Leaks[17]

This section has described the extreme thermal cycles experienced by the cryotanks used on the RLVs and the damage that can occur which can lead to fuel permeation. In order to make composites a viable option for use in this extreme temperature application, further research needs to be conducted to determine a method for increasing the resistance to permeation due to matrix cracking caused by thermal loads.

2.3 Impacts

Another issue surrounding the use of composites on the RLVs cryotanks and feedlines is that these structures are vulnerable to low-velocity impact events. These impact events can damage the composite and lead to fuel permeation. This section will begin with a general description various types of impact testing, then discuss the impact mechanics of composites and the damage mechanisms which can lead to fuel permeation of composite cryotanks and feedlines.

2.3.1 Impact Testing

There are a wide variety of accepted impact tests available to evaluate the various types of impacts, materials, and structures. Different tests simulate various types of impact, whether blunt or sharp, high-velocity or low-velocity. Materials behave differently depending on the type of impact they are subjected to. Therefore, it is important to conduct impacts tests that most closely model the actual types of impacts the material/structure will be exposed to during use, due to the fact that you cannot simply

compare two different impact scenarios and expect the same results unless the entire process is similar.[19] High-velocity impacts, such as runway debris or small arms fire, are generally simulated using a Split Hopkinson-Bar, a gas gun impact or a ballistic projectile. While low-velocity impacts (up to 20 m/s), such as a dropped tool, are generally simulated using a pendulum test (Charpy or Izod), hydraulic test machine, or a drop-weight impact.[20]

To simulate low-velocity impacts, both Charpy and Izod impact test set-up's feature a pendulum arm striking a notched specimen. These tests provide information on the resistance of a material to sudden fracture in the presence of a sharp stress concentration or flaw.[21] Figure 2.3.3 displays the loading configuration of these two tests.

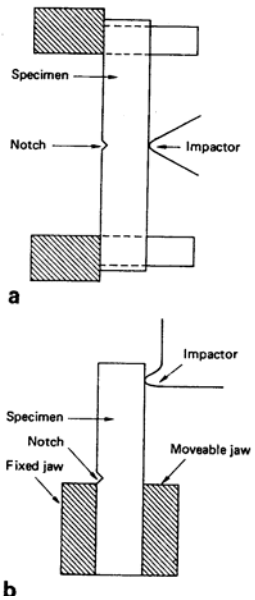

Figure 2.3.1 (a) Charpy and (b) Izod Test Configurations[20]

Unfortunately, these tests are not as useful for modeling the complex behavior of composites, although they work well for metals and isotropic materials. They also do not accurately depict the types of impacts that the RLV's fuel lines will be exposed to.

Another type of low-velocity impact test is a hydraulic test machine. In this type of test, dog-bone or double cantilever beam specimens can be tested over a wide range of strain rates. This technique also permits the evaluation of basic material properties such as tensile strength, modulus and interlaminar fracture toughness.[20] Again, these types of tests are not the most accurate models for the types of impacts experienced by the RLV's fuel tanks and lines.

Drop-weight impact tests, on the other hand, are very useful for modeling the types of impacts experienced by the composite materials on the RLVs, and therefore, this experiment used a drop-weight impact device to determine the impact resistance of the graphite/epoxy composites. These "free flight" drop tower tests, simulate impacts very similar to that which would occur due to a dropped tool. Using various types of impact tips (blunt, hemispherical), known weights are dropped from predetermined heights, which will inflict the desired impact energy. This type of impact test will be described fully in section 4.3 Equipment and Techniques.

2.3.2 Impact Mechanics

These types of low-velocity impacts cause many types of damage within the composite, depending on the amount of impact the specimen is subjected to. Matrix cracking, delamination, fiber/matrix debonding, fiber pullout, and fiber rupture are some of the damage modes caused by low-velocity impacts.[22] Initially, when a composite is

impacted with enough energy, cracks form in the matrix material. Since with PMCs, the matrix is much more ductile than the fibers, upon impact the adhesion between the stiff fibers and the more ductile matrix restricts the matrix from fully deforming as it would without the support from the fibers. In this case, upon impact, cracks form in the matrix material perpendicular to the direction of the fibers.[23] Previous research has also found that impacts that leave no visible damage, may have still caused microcracking.[24] Impacts of high enough energy may cause indentation or crushing of the matrix material, evident by a dent on the surface of the composite at the site of impact. These impacts frequently cause shear stress waves to propagate through the material with enough energy to cause cracking of the matrix material immediately around the site of impact. These surface cracks will be discussed further in section 5.4 Critical Impact Energy.

The next mode of damage is delamination between plies of the composite. This type of damage occurs with higher impact energies than those which caused matrix micro cracking alone.[25] Much of the energy absorbed within a composite upon impact is dissipated through the formation of delaminations. Delaminations seriously jeopardize the compressive strength of the composite and also allow more paths for permeation, which is of particular concern for this research. From a load vs. time plot, one can determine when the delaminations have occurred. The first vertical drop on the plot, typically at around half the maximum load, signifies when the first delamination occurred.

On the bottom side of the specimen, directly opposite the impact, a two lobed shape of a delamination can occur which relates to the difference in fiber angle between plies. The major axis flows along in the direction of the fiber's axis on the bottom layer

of the delamination.[26] Typically when the mismatch angle between two plies is 20° or less, the damage is long and narrow, while as the mismatch angle between two plies increases above 30°, the size of the damage is independent of mismatch.[27]

The next mode of damage is fiber rupture, which will occur following matrix microcracking and delaminations. Fiber rupture occurs on the back face of the specimen, immediately opposite the site of impact on the top face of the specimen. Upon impacting with a high enough energy, the delaminations progress due to high shear stresses ahead of the crack tip which in turn cause more delaminations. The specimen continues to carry load until the fibers in the next layer begin to fail in tension. It is in this manner that the composite laminate can fail. Fibers may rupture on the bottom surface of the specimen due to the increase in tension caused by the deformation of the specimen, while fibers on the top surface may remain intact.[28]

Many attempts have been made to increase the impact resistance of a composite and reduce the damage modes that occur with impacts of various energies. One such example was the attempt to improve the damage resistance by coating the fibers with a tougher sizing to improve the bonding with the matrix material. The reason for this was to avoid the fiber pullout that becomes a significant source of energy dissipation and damage, especially with carbon fiber composites.[20] Unfortunately, these efforts actually reduced the impact resistance of the system because the toughness that originally came from the matrix cracks being diverted along the fiber/matrix interface, was now eliminated, resulting in a more brittle failure than had previously occurred.[23,28]

Although at first thought it seems promising to increase the ductility of the fibers to improve the toughness of the composite, this makes the laminate more rate sensitive.

Under static loading the ductile fibers could withstand more deformation than brittle fibers, but at high strain rates they prematurely rupture because they do not have sufficient time to fully deform.[29]

Toughening the matrix material in a composite with brittle fibers has proved a successful technique for improving impact resistance. These types of toughened epoxy systems exhibit much smaller damage zones than previous non-toughened epoxy systems, providing that the fibers themselves are brittle. These toughened epoxy systems also exhibit an increase in interlaminar toughness by as much as eight times.[30] Two ways to toughen a thermoset polymer include adding a rubbery phase to the polymer or adding some thermoplastic material.[31] Tougher thermoset polymers have an improved ductility due to the slight crosslinking, but their strength is reduced and the polymer can be more permeable.

This section has described the various types of impact tests and the damage mechanisms due to impacting composites which can lead to fuel permeation in applications such as the fuel tanks and feedlines of the NASA's RLVs. In order for composites to be a viable option for the material of the RLVs cryotanks and feedlines, a method must be determined to increase the graphite/epoxy's impact resistance and reduce the likelihood that a low velocity impact will cause fuel permeation.

2.4 Previous Research on Coated and Hybrid Composites

The previous sections have described the effects of thermal cycling and impact events on the permeability of composites. Due to the catastrophic failure associated with

permeation of composites for use on the fuel tanks and feedlines of NASA's RLVs, it has been determined that a method must be devised to improve a graphite/epoxy's resistance to thermal damage and impacts in order for these materials to be a viable option for use in applications of extreme changes in temperature and stresses. The section will describe previous research conducted in this area. Specifically, this section will describe previous research on the effects of surface coatings and embedded barrier layers on the impact and thermal resistance of graphite epoxy composites.

2.4.1 Effects of Surface Coatings

Previous research, conducted by Ben Findley and W.S. Johnson[32] at Georgia Institute of Technology, investigated the effects of surface coatings on the permeability of a graphite/epoxy composite. This research was supported by NASA Marshall Space Flight Center. The objective was to investigate the potential of coatings to improve the impact resistance of carbon/epoxy composites to be used for fuel feedlines and cryogenic tanks on future RLVs. These same coatings were also tested to determine if they could be used to repair composites with preexisting leaks

All composite specimens tested in this research were made from woven IM7 carbon fibers in a matrix of EX1552 (a toughened epoxy). The specimens were cut from 1m by 1m 4-ply panels processed at NASA MSFC, with a $[0/90]_4$ lay-up. Several different commercially available coating materials were considered in this project. An emphasis was placed on testing different polyurethane materials because of both their toughness and also their low permeability. Three different polyurethane materials were considered, an aliphatic moisture curing polyurethane, a polyurethane material reinforced

with micaceous iron oxide and aluminum particles (MIO-Al particles), and a polyester aliphatic urethane. Additionally, two thermoplastic coating materials were considered because they were both marketed as being highly impact resistant with low permeability. Testing was also conducted to show how leakage develops in the coated composite systems with increasing impact energies. All permeability testing was done using a device derived from the volumetric approach outlined in ASTM standard D1434.[33]

This research has shown that polymer-based coatings can be used to improve the impact resistance of carbon/epoxy composites significantly (in this case as much as a 5.5 fold improvement) without experiencing leakage of Helium gas under pressure. Tables 2.4.1 and 2.4.2 demonstrate how the use of these coatings can dramatically increase the critical impact energy of a graphite/epoxy composite.

Table 2.4.1 Critical Impact Energies of Coated Initially Leaking Specimens[34]

Coating	Critical Impact Energy, J (ft*lb)	Improvement Factor
None	1.07 (0.79)	NA
Moisture Curing Aliphatic Polyurethane	5.90 (4.35)	5.51
Polyurethane with MIO-Al Particles	4.31 (3.18)	4.03
Polyester Aliphatic Urethane	5.25 (3.87)	4.90
Thermoplastic	3.12 (2.30)	2.91

Table 2.4.2 Critical Impact Energies of Coated Initially Impermeable Specimens[34]

Coating	Critical Impact Energy, J (ft*lb)	Improvement Factor
None	1.07 (0.79)	NA
Moisture Curing Aliphatic Polyurethane	5.15 (3.80)	4.81
Polyurethane with MIO-Al Particles	3.80 (2.80)	3.54
Polyester Aliphatic Urethane	5.11 (3.77)	4.77
Thermoplastic	3.20 (2.36)	2.99

Although these coatings showed promising results for increasing critical impact energy needed to cause the composite to leak, when cycled to cryogenic temperatures, the coatings all failed to a greater or lesser degree. For this reason, these graphite/epoxy coated composites were deemed unacceptable for use on the fuel tanks and feedlines for NASA's RLVs. It is believed that the polyurethane with MIO-Al particles demonstrated the promise of micro-scale or nano-scale reinforced materials for cryogenic applications. This material survived thermal cycling without visible damage, which means that there was much less damage present in the coating than the other materials.

Results from this research led to the idea of introducing a ductile, thermally compatible layer within the composite to avoid the thermal shock experienced by the surface coatings, in an attempt to improve the graphite/epoxy composite's resistance to damage due to impact and thermally induces stresses. Since this previous research determined that the thermal cycling was the controlling test, for this current project, thermal cycling will be performed first, and the impacting will then be performed on those specimens that passed the thermal cycling. Chapter 4 Experimental Procedures and Equipment, will further discuss the order and motivation for procedural steps followed for this research.

The term "hybrid" composite is not unique to interleaved composites. Composites containing a combination of different fiber types can be referred to as hybrid composites, but for the purposes of this research, a hybrid composite refers to a single fiber type composite laminate with a layer of an isotropic material embedded within the composite during manufacture. An example of a generic lay-up hybrid can be seen in Figure 2.1.5.

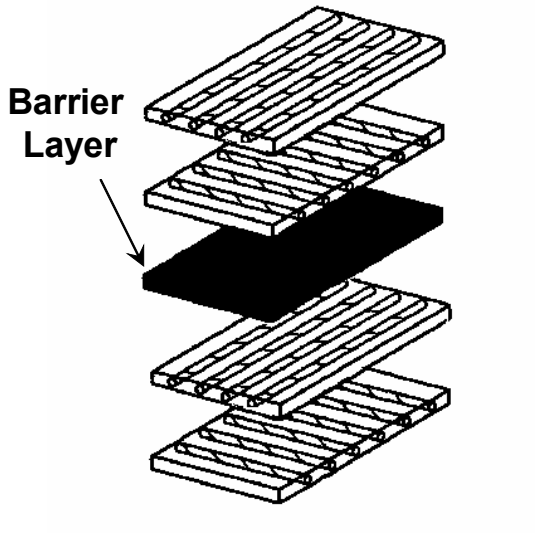

Figure 2.4.1 Generic Hybrid Composite

Composite materials have many advantages over traditional structural materials and their use in industry will certainly continue to increase in the future.

2.4.2 Effects of Composite Interleafing

This section will discuss previous research conducted on the permeability and mechanical behavior of hybrid, or interleaved, composites. Previous research has been conducted on the permeability of hybrid graphite/epoxy composites for proposed use on the LH_2 fuel tank structure. Brian Grimsley *et al* [35], from NASA Langley Research Center, investigated the effects of the addition of various barrier layer materials on the permeability and mechanical properties of an IM7/977-2 composite. This research investigated embedding two commercially available interleaf films and eleven novel LaRC interleaf films, and then tested the permeance of argon at room temperature. The

effects of layer thickness, number of layers, and location of the layers on the mechanical properties of the laminate were investigated.

This experiment investigated Aluminized Mylar®®, self-metallized polyimide, a Vectra film, and an inorganic-organic nanocomposite films. Six eight-ply quasi-isotropic $[0/90/45/-45]_s$ lay-up control panels were fabricated and composites containing various interleaf materials were also fabricated. The panels with the interleaf film layer were examined using the pulse-echo C-Scan technique and found to be acceptable. Permeability characterization of the films and interleaf composites was performed in accordance with ASTM D-1434.[33] From the results of these tests, the Polyimide Hybrid was the most promising of the non-metallized barrier layer because of its low permeance. The film with the lowest permeance was the Aluminized Mylar®. The control composite itself was found to have a lower permeance than most of the films. Only the hybrid composites containing Mylar® and phenoxy with clay were found to show an improvement in permeance as compared to the control.

To determine mechanical properties, twelve unidirectional composite panels were fabricated containing aluminized Mylar® films of 6μm(.25mil), 25.4 μm (1mil), and 102 μm (4 mil) thicknesses. Most of the panels were fabricated with the interleaf inserted as the middle ply, while others were fabricated with three layers of the 25.4 μm (1mil) inserted upon fabrication as follows, $[0_3/\text{film}/0_2/\text{film}/0_2/\text{film}/0_3]$ or $[0_5/\text{film}/0_5/\text{film}/0_5/\text{film}/0_5]$ for the 10 ply and 20 ply lay-ups respectively. The 20-ply specimens were subjected to short beam shear (SBS) tests and the 10-ply specimens were subjected to flexure tests. The interleaf panels exhibited a 50% reduction in SBS strength and up to a 20% reduction in flexural modulus as compared with the control.

The composite panel with three interleafs exhibited the lowest shear strength but interestingly, was found to have the highest flexural modulus. Both the flexural strength and modulus were found to increase with decreasing film thickness. Under the SBS tests and the 0° flex tests all specimens were found to have failed at the interface between the aluminum and Mylar®, rather than at the aluminum to epoxy interface. The strength of this Mylar®-aluminum bond must be improved in order for this type of hybrid composite to be used for these applications.

Previous work, conducted by Humpenoder[36], investegated fiberglass and carbon/epoxy composites containing either aluminum foil or tin foil to determine the effects of mechanical and thermal cycling on permeability. This experiment measured the permeability of helium, hydrogen, and methane. Initially, the temperature dependence of permeability was investigated and results show that as the temperature drops, the permeability of the specimens dropped. The control composites were subjected to mechanical cycles under four point bending at room temperature and LN_2 (-196°C) until a reduction in bending modulus was observed. Those specimens mechanically cycled at the cryogenic temperature exhibited 30% increase in the permeation parameter. Measures of permeation versus temperature also showed that the permeation decreases with decreasing temperature. Thermally cycling these specimens 100 times down to (-196°C) was shown to have a negligible effect on permeation.

Next the interleaf specimens containing aluminum foil or tin foil were subjected to the same series of tests. Humpernoder[36] found that these interleaf specimens exhibited negligible permeability. Upon thermal and mechanical cycling, the composites

containing aluminum foil delaminated at the aluminum-composite interface. The composites containing tin foils exhibited excellent adhesion.

Previous research has been conducted by Robert Evans and John Masters[37] on toughening graphite/epoxy composites by embedding thin layers of tough, ductile material within a graphite/epoxy composite system. This research investigated the effects of the addition of an interleaf material on the residual compression strength after impact and hot/wet compression strength. Since much of the delamination failure of a composite is controlled by its inability to undergo shear deformation, tough interleaf materials were embedded within the composite to improve its toughness. It was found that these hybrid composites exhibited an increase in impact resistance, i.e., smaller and less damage was observed with the C-scans. This research found that this interleafing is most effective when combined with a tougher matrix system. Significant increases in composite damage tolerance were found with the addition of interleaf material. The hot/wet compression test results indicate that the increase in impact resistance does not come at the expense of structural performance. The hybrid composites exhibited a slight decrease in strength compared to the controls, and these reductions obey the rule of mixtures approximation.[38] A substantial increase in compression after impact results of interleafed composites was attributed to the reduction in delamination size due to the addition of the interleaf layer. The results and lessons learned from previous research on hybrid composites was used to determine the best approach for this current project on investigating the permeability behavior of interleafed composites under thermal loads and low-velocity impacts.

CHAPTER 3 MATERIALS

This chapter will describe the materials investigated for this research. The composite's constituent properties will be discussed, as well the mechanical properties of the candidate barrier layers.

3.1 Composite Constituents

The composites specimens for this research were manufactured using a unidirectional prepreg of IM7 graphite fibers embedded in a 977-2 toughened epoxy matrix. These are the same constituents used for the composites of the face sheets of the LH2 propellant tank for the X-33.[35] This section will discuss the properties of the fibers and the matrix. The lay-up and processing of the composite laminate will be discussed further in section 4.3.1 Autoclave.

3.1.1 Fibers

The fibers used in the composites for the face sheets of the X-33 cryogenic fuel tank were IM7 carbon fibers.[35] Therefore, the composite specimens investigated for the purposes of this research were also manufactured with these continuous, high performance, and intermediate modulus, IM7 fibers. These fibers are produced by Hexcel Composites, and are available in 6000 or 12,000 filament count tows. It is unknown which was used in the prepreg supplied for this research. The fiber has been surface treated and can be sized to improve its interlaminar shear properties, handling

characteristics, and structural properties. These fibers are PAN based, and have extremely low densities and high strength, as opposed to PITCH based carbon fibers which have extremely high moduli at the expense of extremely high strength. These fibers are very anisotropic and exhibit much lower mechanical properties in the transverse direction.

Due to their unique combination of properties of the IM7 fibers, such as higher tensile strength and modulus, as well as good shear strength, using these fibers, designers can achieve higher safety margins for both strength and stiffness critical applications. The properties of the Hexcel IM7 fibers are displayed below in the Table 3.1.1, followed by Tables 3.1.2 and 3.1.3 displaying additional mechanical properties of IM7 fibers.

Table 3.1.1 Properties of Hexcel IM7 Fibers[39, 40]

Fiber Type	Strength, σ MPa (ksi)	Modulus, E MPa (Msi)	Strain to Failure (%)	Carbon Content (%)	Density N/cm3 (lb/in3)
IM7 (5000) 6K	5170 (750)	275900 (40.0)	1.87	94	0.0176 (0.0643)
IM7 (5000) 12K	5520 (800)	275900 (40.0)	2.00	94	0.0176 (0.0643)
IM7 (6000) 12K	5760 (835)	289700 (42.0)	1.99	94	0.0177 (0.0646)

Table 3.1.2 IM7 Fiber Mechanical Properties[41]

E_{11}	E_{22}, E_{33}	v_{12},v_{13}	v_{23}
263.7 GPa	19.0 GPa	0.20	0.35

Table 3.1.3 IM7 Fiber Mechanical Properties[42]

α_{11}	α_{22}, α_{33}	σ_{lt}	σ_{lc}	G_{12}, G_{13}	G_{23}
-9.00E-07	7.20E-06	2.86 GPa	2.53 GPa	27.6 GPa	6.89 GPa

3.1.2 Matrix

The matrix material used for this research was a Cycom® 977-2, which is the same material used in the face sheets for the LH_2 propellant tank.[35] This material is a 177°C (350°F) during toughened epoxy resin with a 126-138°C (260-280°F) dry and 104°C (220°F) wet service capability. This matrix material is formulated for autoclave or press molding. Typical applications for this 977-2 include aircraft primary and secondary structure, space structure, ballistics, cryogenic tanks, or any application where impact resistance and light weight are desired.[42] Mechanical properties for this 977-2 can be found below in Tables 3.1.4 and 3.1.5.

Table 3.1.4 Properties of 977-2 Epoxy Matrix (Cytec)[42]

	RT
Tensile Strength, ksi	11.8 ± 1.6
Tensile Modulus, Msi	0.51 ± 0.02
Tensile Strength, MPa	*81.4 +/- 11*
Tensile Modulus, GPa	*3.52 ± O. 14*
Flexural Strength, ksi	28.6 ± 1.0
Flexural Modulus, Msi	0.50 ± 0.01
Flexural Strength, MPa	*197+/- 7*
Flexural Modulus, GPa	*3.45 +- 0.07*
G_{1c}	
in-lb/in^2	2.73 ± 0.48
J/m^2	478 ± 84
K_{1c}	
MPa • m$^{1/2}$	*1.34 ± 0.15*
ksi • in.$^{1/2}$	*1.22 ± 0.14*
Tg, °C (RDS, 10°C/min)	212
Density, g/cc	1.31

Table 3.1.5 Properties of 977-2 Epoxy Matrix (Sankar)[42]

E	3.32 GPa
v	0.35
CTE	5.76E-05
Tensile Strength	86.9 MPa
Compressive Strength	119 MPa
G	1.23 GPa
Shear Strength	86.9 MPa

3.2 Barrier Layer Materials

This section will begin with a discussion of the initial evaluation of potential barrier layer materials, discuss the properties of each of the chosen barrier layer materials and compare the advantages and disadvantages of each barrier layer.

3.2.1 Barrier Layer requirements

Before any hybrid composites were manufactured, an evaluation of potential barrier layer materials was performed. Only those materials with low densities (and/or the ability to be manufactured into thin sheets) and those with sufficient toughness were even considered. The list of potential barrier layer materials were then narrowed down using the additional requirements as described below:

- have a cure temperature at or below that of the matrix material
- be thermally compatible enough with the composite to endure extreme ΔT
- be tough enough to withstand low velocity impacts

- have sufficient low temperature toughness to resist cracking
- adhere well enough to not reduce interlaminar toughness of the composite
- be durable enough to withstand long service life

One potential candidate was a PETI-5 material. As reported in his Master's thesis, Matt Pavlick[43] described how PETI-5 has been shown to have attractive properties for adhesive and matrix material applications. Unfortunately, it was determined that these Phenylethynyl-terminated polyimides require high temperature treatment to completely cure. These cure temperatures for PETI -5 are on the order of 260°C, which is high enough to degrade the 977-2 matrix which has a cure temperature of 212°C. Therefore, this material was eliminated as a possible barrier layer candidate.

Another, potential candidate was tin. Research conducted by Humpernoder [36] determined that tin embedded within a graphite/epoxy and fiberglass composite exhibited excellent adhesion and negligible permeability. Due to its relatively high ductility and ability to be manufactured into thin sheets, this material initially seemed a good option for a barrier layer material. Unfortunately, upon further investigation, it was found that Tin degrades when exposed to low temperatures. This degradation is due to a change in crystal structure from body-centered tetragonal (BCT) to diamond cubic (DC) structure at low temperatures. This cooling causes internal expansion which can cause internal stresses which can lead to failure of the material.[44]

After an initial evaluation, the following candidates were chosen to embed within the graphite/epoxy composite: aluminized Mylar®®, aluminum foil, and two -Titanium films. These materials will be discussed in the following sections of this chapter.

3.2.2 Aluminized Mylar®

Two thicknesses of aluminized Mylar®(a DuPont trade name) were chosen to embed within the composite laminate: one 6 µm layer and one 50 µm layer. The material used for this research was donated by Lambda Inc. and was manufactured by Alexander Vacuum. Mylar® is a commercial polyester, poly(ethylene terephthalate), or PET. Other common trade names for this polymer include: Dacron, Fortrel, and Terylene.[44] Aluminized Mylar® is composed of a thin layer of polyester with a vacuum deposited layer of aluminum on both sides and overcoated on both sides with a heat sealable PVDC copolymer. This film has excellent oxygen, moisture, and light barrier properties.[45] Table 3.2.1 displays various mechanical and thermal properties of this material.

Table 3.2.1 Properties of 14µm Aluminized Mylar®

Density, g/cc	1.4
Film Tensile, MPa	165
Film Elongation at Break, %	100
Modulus of Elasticity, GPa	3.45
Tear Strength	300
Seal Strength, g/25 mm	201
Max Service Temperature, °C	121

Data indicates that mechanical properties show a slight increase with an increase in thickness of the film. Mylar® polyester film retains it's physical properties over a large range of temperatures and is useful at temperatures ranging from -250°C to 200°C when the physical demands are not high.[35] Its relatively low density and ability to be manufactured into extremely thin sheets, as well as its high ductility, and large range of

usage temperatures, make Aluminized Mylar® an excellent candidate for barrier layer material.

3.2.3 Aluminum Foil

Two thicknesses of 1100 Aluminum foil were chosen to embed within the composite laminate: one 16 μm layer and one 35 μm layer. The Aluminum foil chosen for this research was manufactured by Alcoa, the thin sample was Standard Reynolds Wrap and the thicker sample was Extra Heavy Duty Reynolds Wrap. Table 3.2.2 displays manufacturer's mechanical data for 1100 Aluminum foil. Table 3.2.3 displays physical, mechanical and thermal properties of 1100 Aluminum found on MatWeb.[45]

Table 3.2.2 Reynolds Wrap 1100 Aluminum Foil Data[46]

Gauge	Gauge	Ten-sile	Ten-sile	Elonga-tion	Pin-holes per Sq. Ft.	Pin-holes per Sq. Meter	Mullen
		Strength	Strength				Burst
Micron	*Inches*	*KSI*	*MPa*	*%*	*Typ.*	*Typ.*	*Typ.*
12.7	0.0005	9 to 12	62 to 83	2 to 5	<1	<11	7
15.2	0.0006	9 to 12	62 to 83	2 to 6	<1	<11	9
16.5	0.00065	9 to 12	62 to 83	2 to 6	<1	<11	10
17.8	0.0007	9 to 12	62 to 83	3 to 6	<1	<11	11
20.3	0.0008	9 to 12	62 to 83	2 to 7	<1	<11	14
22.9	0.0009	9 to 12	62 to 83	3 to 7	<1	<11	16
25.4	0.001	9 to 12	62 to 83	3 to 7	*	*	19
30.5	0.0012	9 to 12	62 to 83	4 to 9	*	*	25
40.6	0.0016	9 to 12	62 to 83	6 to 10	*	*	38
45.7	0.0018	9 to 12	62 to 83	6 to 12	*	*	46
50.8	0.002	9 to 12	62 to 83	7 to 13	*	*	54
63.5	0.0025	9 to 12	62 to 83	8 to 14	*	*	75
76.2	0.003	9 to 12	62 to 83	10 to 17	*	*	99
88.9	0.0035	9 to 12	62 to 83	11 to 19	*	*	124
101.6	0.004	9 to 12	62 to 83	12 to 22	*	*	152
114.3	0.0045	9 to 12	62 to 83	13 to 23	*	*	181
127	0.005	9 to 12	62 to 83	14 to 25	*	*	212
139.7	0.0055	9 to 12	62 to 83	14 to 27	*	*	245

* Aluminum Foil over .001" (25.4 µm) is considered to be pinhole free

Table 3.2.3 Properties of 1100 Aluminum Foil[45]

Density, g/cc	2.71
Hardness, Brinell	23
Tensile Strength, Ultimate, MPa	90
Tensile Strength, Yield, MPa	35
Elongation at Break, %	35
Modulus of Elasticity, GPa	69
Poissons Ratio	0.33
Shear Modulus, GPa	26
Shear Strength, MPa	60
Compressive Modulus, GPa	70.4
CTE, linear 20°C, µm/m-°C	23.6
CTE, linear 250°C, µm/m-°C	25.5

Aluminum foil was considered a promising barrier layer material because of its relatively high ductility as well as its low temperature properties. Most aluminum alloys perform extremely well even down to the most extreme temperature ranges. Aluminum has a FCC (face center cubic) crystal structure and no ductile-to-brittle transition; therefore they are known to retain their toughness even at very low temperatures. Below zero most aluminum alloys show little change in properties, yield and tensile strengths may increase, elongation may decrease slightly, but impact strength remains approximately constant.[47] These properties make aluminum prime candidates for cryogenic applications, and therefore superior barrier layer candidates for the purpose of this research.

3.2.4 β – Titanium Foil

Two types of β-Titanium foils were chosen as barrier layer materials for this project. One foil was sent from NASA and was a β-Titanium 15-3 uncoated film of thickness 152μm. The second foil was sent from Boeing and was a 127μm thick, β-Titanium 15-3-s foil coated with a resin to assist the foil in adhering to the composite. The 15-3 denotation relates to the amount of each component present in this alloy. Table 3.2.4 describes the composition of this particular alloy.

Table 3.2.4 Material Make-Up of β-Titanium 15-3

Component	Value
Aluminum, Al	3
Chromium, Cr	3
Tin, Sn	3
Titanium, Ti	76
Vanadium, V	15

Titanium is known for its high strength and good ductility and has a HCP (hexagonal close-packed) crystal structure. An interesting point to note about titanium is that, the grains can become rotated during rolling which can result in anisotropic behavior. This means that properties such as strength and ductility can be different depending upon the direction they are measured in relation to the rolling direction.[44]

Another important point to mention about titanium for use in applications for cryogenic LH_2 tanks, is that titanium can be particularly vulnerable to hydrogen embrittlement. The presence of hydrogen and oxygen can lead to deterioration of titanium which can cause a decrease in mechanical strength. Particularly common with HCP alloys, hydrogen can react with the metal to produce a brittle hydride phase.[44]

Titanium can also exhibit very different mechanical properties depending upon its heat treatment. The β-Titanium 15-3 resin coated foil sent from Boeing was solution treated at 1450°F for 10 minutes and then rapid argon cooled to 600°F. It was intended to maintain beta phase. Preliminary results from testing underway by Mathew Hammond and Dr. W.S. Johnson suggest that this type of heat treatment will drastically reduce the modulus of the titanium. The β-Titanium 15-3 no resin foil sent from NASA was solution treated 788°C (1450°F) – 816°C (1500°F) and then air cooled to 510°C (950°F)

over an 8 hour time period. Preliminary results from testing suggests that this heat treatment of titanium would exhibit a higher modulus than the previously mentioned rapidly quenched titanium, closer to the value of the as received titanium samples.

Unfortunately, there is very little data available on the effects of different heat treatments on this particular β-Titanium 15-3. Table 3.2.5 displays various physical, mechanical, and thermal properties of different heat treatments of β-Titanium 15-3 found from MatWeb's online database.[45]

Table 3.2.5 Properties of Various Heat Treatments of β-Titanium 15-3

β-Ti 15-3-S Properties	Solution Treated	Annealed	Aged 545°C	Aged 510°C
Density, g/cc	4.76	4.94	4.76	4.76
Tensile Strength, Ultimate, MPa	790	915	1110	1340
Tensile Strength, Yield, MPa	770	880	1010	1210
Elongation at Break, %	22	15	13	8
Modulus of Elasticity, GPa	82	83	100	100
CTE, linear 20°C, µm/m-°C	8.5	7.07	8.5	8.5
CTE, linear 250°C, µm/m-°C	9.1	8.9	9.1	9.1
CTE, linear 500°C, µm/m-°C	9.8	9.5	9.8	9.8

Although there are a few concerns with using titanium for this application, there are many possible benefits of using this material as a barrier layer with in a graphite epoxy laminate. One advantage of using titanium as a barrier layer in this application is its low coefficient of thermal expansion. The composite itself has a low CTE, so having a smaller difference in CTE between the composite and barrier layer will mean that less thermal stresses will build up in the laminate upon thermal cycling. Another benefit of

titanium is its extremely high strength and good ductility. This high strength should allow the titanium barrier layer to remain intact upon impact even when the composite itself has been damaged. Titanium foils are also currently used within composites to improve the bearing stress resistance. For these reasons, the titanium foils are excellent barrier layer candidates for the purposes of this research.

3.2.5 Barrier Layer Comparison

This section will compare the properties of the three chosen barrier layers and discuss the advantages of each. Table 3.2.6 displays a comparison between various mechanical and thermal properties of each barrier layer. These properties are subject to variability due to heat treatment and thickness of each layer, but this table provides a baseline comparison between trends in these barrier layer material properties.

Table 3.2.6 Barrier Layer Material Property Comparison[45]

Property	Al foil	B-Ti	Al Mylar
E_A (GPa)	69	83	3.79
v (Poisson ratio)	0.33	0.33	0.33
CTE (μm/m-ºC)	25	7.07	60
σ_{yield} (MPa)	35	880	55
$\sigma_{ultimate}$ (MPa)	90	915	180

It can be seen that the modulus of the Aluminum foil and β-titanium are comparable, while the modulus of the Mylar® is much lower. The ultimate strengths of

the Aluminum foil and the Mylar® are comparable, while the β-titanium is very much stronger.

Another concern with any material embedded within the graphite/epoxy composite is that it not add a significant amount of weight to the structure. Table 3.2.7 displays a comparison of the barrier layers by the weight added per area. Due to the fact that each layer has a different thickness, comparing densities is not sufficient in this case.

Table 3.2.7 Weight per Area Comparison of Barrier Layer Materials

Film Type	Density kg/m^3 (lb/ft^3)	Thickness μm (mil)	Weight/Area kg/m^2 (lb/ft^2)
Al Mylar (thin)	1400 (87)	6.00 (0.20)	8.4E-03 (0.001)
Al Mylar (thick)	1400 (87)	50.0 (2.00)	7.0E-02 (0.014)
Al Foil (thin)	2710 (169)	16.0 (0.60)	4.3E-02 (0.008)
Al Foil (thick)	2710 (169)	35.0 (1.40)	9.5E-02 (0.020)
β-Ti (no resin)	4760 (297)	152 (6.00)	7.2E-01 (0.148)
β-Ti (resin)	4760 (297)	127 (5.00)	6.0E-01 (0.124)

It can be seen that the Mylar® and Aluminum foil add very little weight per area, while the β-titanium films, due to their increased density and thickness, add a significantly greater weight per area, an order of magnitude greater than the other two materials.

CHAPTER 4 EXPERIMENTAL PROCEDURES AND EQUIPMENT

This chapter will begin with a description of the procedural steps followed for this experiment. Next, the various tools of analysis will be explained and finally, the equipment and testing procedures will be described in detail.

4.1 Procedure

This research was executed in several distinct and sequential phases. Because of the nature of the experiments and the results sought, the order in which the testing was performed was of utmost importance. The following sections will briefly describe each step.

4.1.1 Step I. – Evaluate Potential Barrier Layers

The first step was to conduct an investigation into potential barrier layer materials as described previously in Chapter 3 Materials. Only those materials with low densities (and/or the ability to be manufactured into thin sheets) and those with sufficient toughness were even considered. The list of potential barrier layer materials were then narrowed down using the additional requirements described previously in Chapter 3.

4.1.2 Step II. – Manufacture Hybrid and Control Composites

The next step was to use an autoclave to manufacture hybrid composite laminates containing the best candidate films. Control composites without a barrier layer were also fabricated. The control composites were manufactured with a $[0/90]_{2s}$ lay-up. The hybrid composites were manufactured with the same lay-up, but with the addition of the barrier layer as the middle ply. Figure 4.1.1 and Figure 4.1.2 depict the lay-up of both the control and hybrid composites.

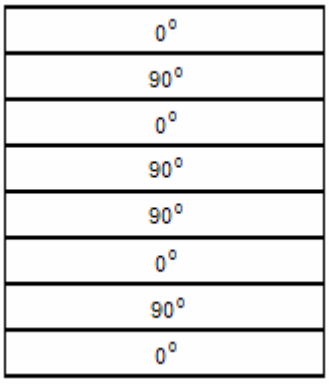

Figure 4.1.1 Control Lay-Up

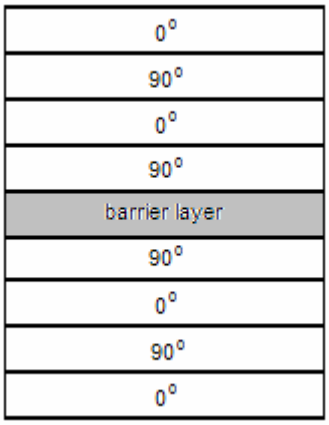

Figure 4.1.2 Hybrid Lay-Up

4.1.3 Step III. – Leak Test Hybrid and Control Composites

Because it has been found that some sample feedlines have actually had leakage prior to any impact events or thermal cycling[8], it is necessary to determine if this method of manufacture will allow a higher percent of composite structures to be leak-free after manufacture. In order to determine if this method of fabrication was successful (i.e. hybrid composites are leak-free), both hybrid composites and control composites (without an embedded barrier layer) were then leak tested with pressurized Helium.

4.1.4 Step IV. – Subject Composites to Thermal Cycling

Due to the mismatch of CTE of the fibers and the matrix, large temperature changes result in significant stresses in the composite which can cause matrix micro-cracking that can lead to fuel permeation. Based on previous research conducted by Dr. W.S. Johnson and Ben Findley[10] at Georgia Tech, it was determined that the thermal cycling would be the controlling test, because all coated specimens failed during thermal cycling. Therefore, for this research, thermal cycling of the specimens was performed before attempting to determine their critical impact energy, as a screen to prevent those specimens previously determined unviable due to their degradation upon thermal cycling, from going on to further testing. Therefore, control composites and as well as those hybrid composites that proved to be leak-free after manufacture, were then subjected to thermal cycling. Damage caused by thermal cycling into the cryogenic range has been found to accumulate quickly, with the maximum crack density of carbon/epoxy composites generally being reached within five cycles.[17] Therefore, the composite specimens were thermally cycled five times, each cycle consisting of 20 minutes at a low

temperature using LN_2 (77K), 20 minutes at room temperature, 20 minutes in an oven (400K), then 20 minutes at room temperature again.

4.1.5 Step V. – Leak Test Composites

In order to determine the degree of damage caused by the thermal cycling, all hybrid and control specimens were then leak tested again.

4.1.6 Step VI. – Determine Critical Impact Energy of Composites

Because the fuel tanks and feed lines are vulnerable to low-velocity impacts, such as those due to dropped tools or inadvertent bumping, it was necessary to determine if the addition of a barrier layer would increase the amount of impact the composite can withstand without leaking. The control composites as well as those types of hybrid composites that proved to be leak-free after thermal cycling were subjected to a series of impact tests in order to determine their critical impact energy (CIE). Also, those specimens which had undergone thermal cycling were then put through the impact tests to determine the effect of thermal cycling on CIE. The CIE is defined as the maximum amount of impact that the composite can withstand without leaking.

4.1.7 Step VII. – Thermal Cycle Impacted Specimens

The fuel tanks and fuel lines will be expected to withstand multiple flights. It is a possibility that an impact could occur in between flights, damaging the material, but not quite causing it to leak. Upon subsequent flights (i.e. additional thermal cycling), the

area of impact could be further damaged, leading to fuel permeation. For this reason, sample specimens of each type that had been impacted close to the CIE, but who were not leaking, were then subjected to thermal cycling.

4.1.8 Step VIII. – Leak Test Impacted/Thermally Cycled Specimens

Those specimens that had been impacted then thermal cycled, were then leak tested to determine if the accumulated damage was sufficient to cause fuel permeation.

4.2 Equipment and Techniques

The primary equipment used in this investigation consisted of an autoclave, leak testing equipment, thermal cycling equipment, and a drop-weight impact machine. The following sections will describe, in detail, the testing equipment itself, as well as the experimental procedures associated with each test.

4.2.1 Autoclave

All specimens investigated were manufactured at Georgia Tech using an autoclave. An autoclave is a closed vessel that permits application of pressure and heat and is used for curing composites. The autoclave used for this research belongs to the composites processing lab in the Aerospace Engineering building at Georgia Tech. This autoclave was manufactured by the American Autoclave Company. Figure 4.3.1 displays the autoclave used to manufacture these specimens.

Figure 4.2.1 Autoclave

The first step in manufacturing a laminate is to cut the plies from the roll of unidirectional graphite/epoxy prepreg. The mold was 12” x 16”, so due to the desired lay-up of the composite, plies are cut with appropriate dimensions so that when placed on top of one another the fibers would lay at the correct angle. The Figure 4.3.2 displays the roll of prepreg being marked to be cut.

Figure 4.2.2 Cut Plies from Prepreg

Once the plies are cut to the appropriate dimensions, they are then placed-up atop one another, one by one, in the correct order. The control composites were manufactured with a $[(0\ 90)_{2s}]$ lay-up. The hybrid composites were manufactured with the same lay-up, but with the addition of the barrier layer as the middle ply. The barrier layer films were cleaned using acetone before being placed in the lay-up, to ensure the best possible adhesion with the composite itself. After each ply is placed down, a rolling pin was used to flatten the laminate as shown below in Figure 4.2.3.

Figure 4.2.3 Lay-up Prepreg Plies

After lay-up, the laminate is placed in a greased mold and covered on both the top and the bottom by releasing film to keep the mold as clean as possible. Breather material, felt, is then placed around the edges of the mold and underneath the vacuum connection hardware. Next, a double-sided tape is placed around the edges of the mold, and the vacuum bag material carefully applied to properly seal the mold as shown below in Figure 4.2.4.

Figure 4.2.4 Seal Laminate in Mold with Vacuum Bag

Finally, the mold is placed in the autoclave and a vacuum applied. The laminate is then subjected to the manufacturer's suggested cure cycle, provided below in Figure 4.3.5. The temperature and pressure are ramped up from room temperature and 0 psi to 350 °F and 85 psi over an hour time period. The laminate is then held at these conditions for 3 hours, and finally the temperature and pressure are ramped down to 72 °F and 0 psi over an hour time period.

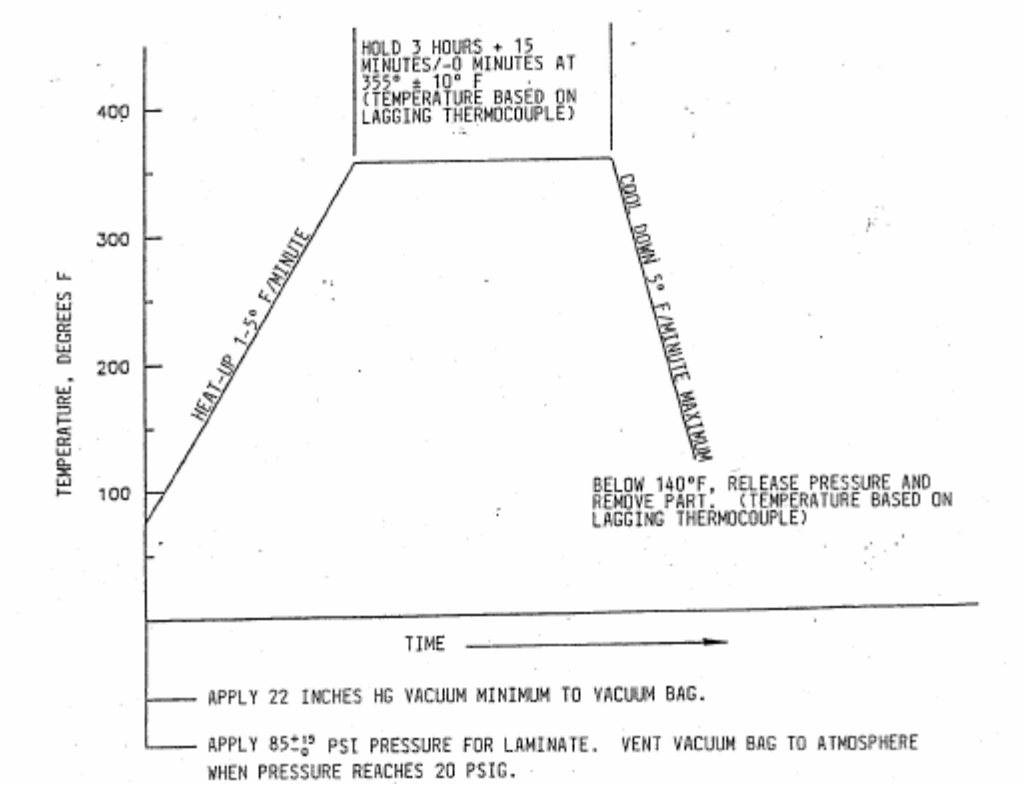

Figure 4.2.5 Epoxy Manufacturer's Cure Cycle

When the cure cycle has completed, the mold is removed from the autoclave and the laminate is removed from the mold and visually inspected for any abnormalities. Assuming the panel is determined to have been properly cured and the vacuum bag properly sealed, the panel is then marked off into 12- 4"x4" grids. Each square is then labeled according to the type of composite and panel number, as well as position within the panel. The Figure 4.2.6 displays the spatial numbering of the panel.

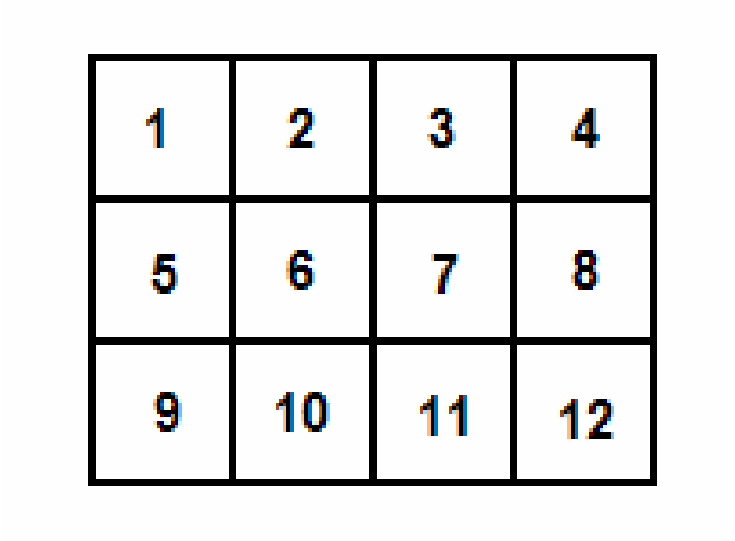

Figure 4.2.6 Specimen Numbering of Laminate Panel

Panels were numbered in case a high variation of material behavior was observed within one panel, it could then be determined how/if the position of the specimen within the laminate effected the it's properties. Finally, a wet tile saw, property of the Composite Research Center (CRC) at Georgia Tech, is used to cut the panel into 12 4"x4" samples.

4.2.2 Leak Test Equipment

The purpose of this leak test was simply to determine whether or not the specimen was leaking, not to quantify the rate of permeation. The leak testing equipment used in this investigation was based on an apparatus developed previously at NASA MSFC[8] and was built by Ben Findley while conducting research at Georgia Tech. The leak test apparatus from NASA MSFC is displayed in Figure 4.2.7.

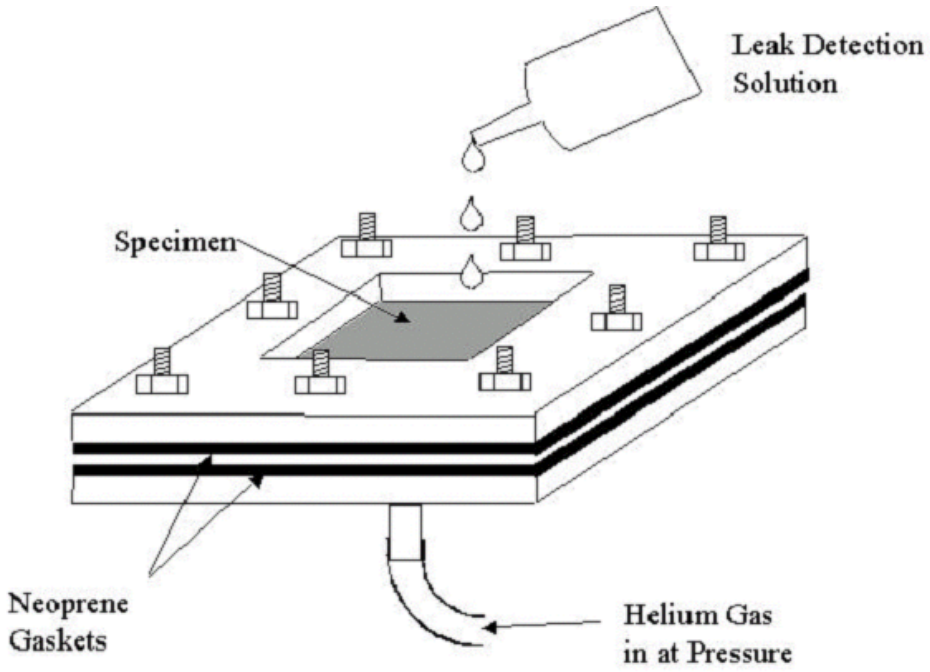

Figure 4.2.7 NASA MSFC Leak Detection Apparatus

The leak test equipment used in this research was geometrically slightly different than the apparatus used at NASA MSFC. Instead of having square holes in the aluminum plates, circular holes were machined in the top and bottom aluminum plates. Damage caused by impacts radiate outward, therefore it was determined that circular holes would make the most sense. Another advantage of circular holes is that, unlike square holes, there are no corners at which maintaining a proper seal would be difficult. Due to fact that the specimens used in this research were slightly larger than those investigated at NASA MSFC, the sides of leak detection equipment used at Georgia Tech were machined 1" longer (from 5" to 6"). The plates were built out of 6061 aluminum and the mutli-view pictures of the top and bottom plate can be seen below in Figure 4.3.8 and Figure 4.2.9.[10]

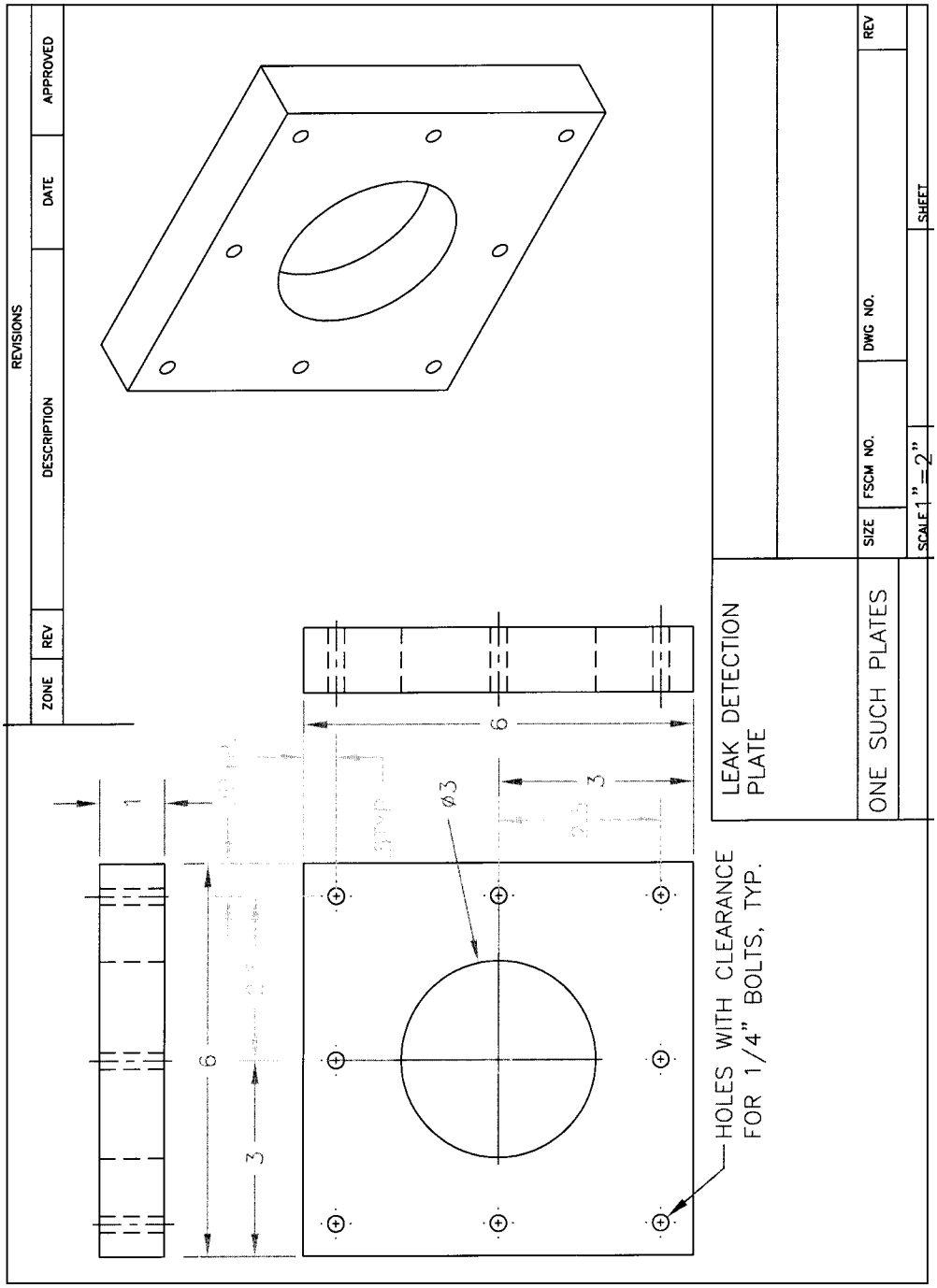

Figure 4.2.8 Multi-View of Leak Detector's Bottom Plate[10]

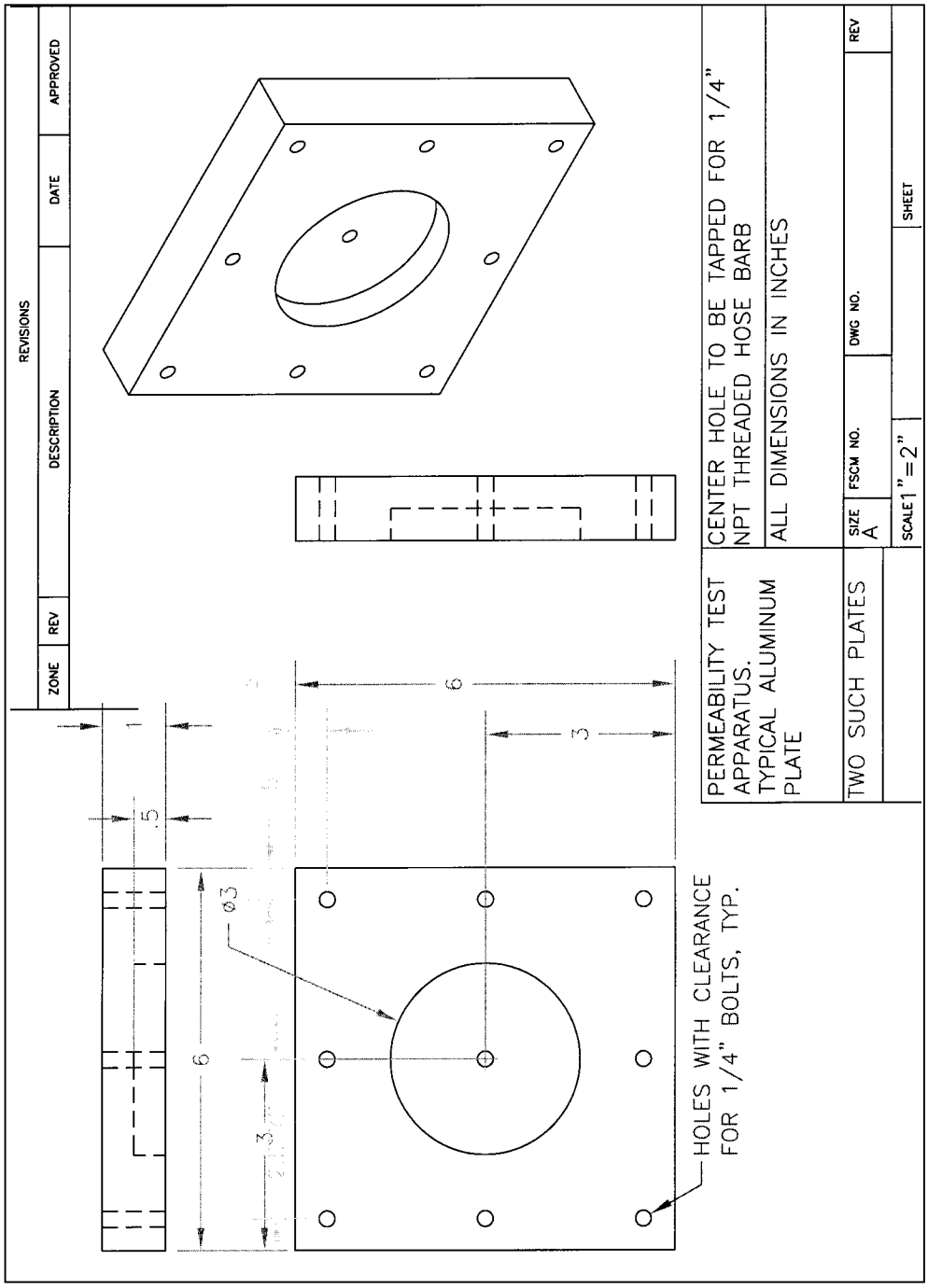

Figure 4.2.9 Multi-View of Leak Detector's Bottom Plate[10]

To begin the leak test, the apparatus was secured on a 4”x4” stand, built in house. In order to ensure that pressurized Helium was applied directly to the specimen and not leaking between the specimen and the gaskets, vacuum grease was applied to the faces of the gaskets to be in contact with the specimen. The specimen then was placed on top of the lower gasket and aluminum plate, and centered on the hole. The specimen was then enclosed by the top gasket and aluminum plate, and the eight bolts were tightly clamped down using a wrench. The circular hole in the top plate was then filled with approximately 3 ounces of a leak detection solution (consisting of two drops of liquid dish soap and water). This leak detection solution was used to ensure that any leaks would be clearly visible and would appear as a stream of bubbles originating from the top surface of the specimen. Pressurized Helium was then applied through the bottom plate, and was slowly increased up to 30 psi, which is the expected pressure in the feed lines. Acceptable rates of permeation for both liquid oxygen and liquid hydrogen are extremely low, so for the purposes of this research, any identifiable leaks were considered impermissible. If no leaks were observed during the application of 30 psi pressurized Helium, the specimen was recorded as “leak free”. If leaks were observed, the pressure at which the specimen started leaking, the number of leaks, and the severity of the leak(s) were recorded.

4.2.3 Thermal Cycling Equipment

Due to the mismatch of CTE between the fibers, matrix, and barrier layer material, large changes in temperature produce significant stresses within the composite that can cause matrix microcracking which can allow the laminate to leak. In order to

determine if the addition of the barrier layer allowed the composites withstand the stresses induced by the large change in temperature, specimens were subjected to extreme thermal cycling.

To begin, holes were drilled in each of the four corners of those specimens that had been chosen to undergo thermal cycling. In order to ensure that the drilling did not cause damage, the specimens were backed with plywood during drilling. The specimens were then strung together with thermo-couple wire in stacks of up to nine samples. Thermocouple wire was used simply because of its ability to withstand extreme temperatures without degrading. Figure 4.2.10 displays a stack of samples ready for thermal cycling.

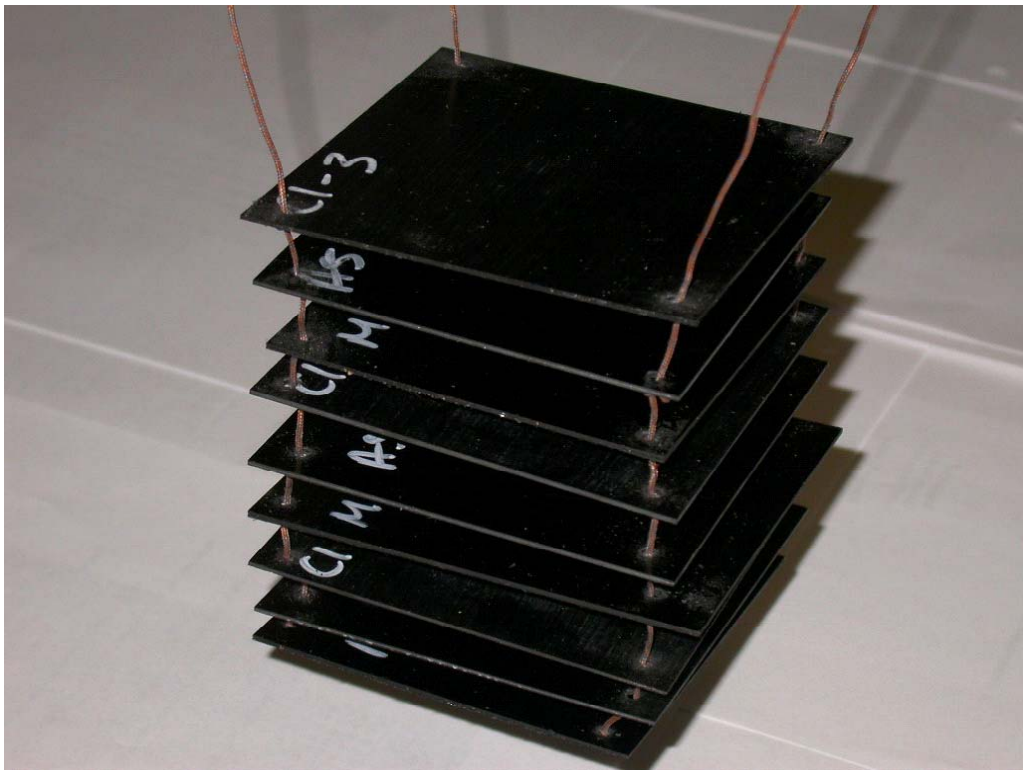

Figure 4.2.10 Specimens Prepared for Thermal Cycling

The first step in the thermal cycling is to simulate the cryogenic temperatures experienced by the fuel tanks and fuel lines when the tanks are fully fueled with LH_2 and LO_2. To accomplish this, the stack of specimens were submerged in LN_2, which causes the temperature of the specimens to drop to -196°C (320°F) The stack is submerged in the cryogenic liquid for 20 minutes. Figure 4.2.11 displays a stack of specimens submerged in LN_2.

Figure 4.2.11 Specimen Submerged in LN_2

After the specimens have been submerged in LN2 for 20 minutes, they are removed and held at room temperature to thaw out for 20 minutes. The following figure

displays a picture of the specimens immediately after their removal from the cryogenic liquid. It can be seen that the specimens have frosted over. This condensate quickly evaporates as the specimens reach room temperature.

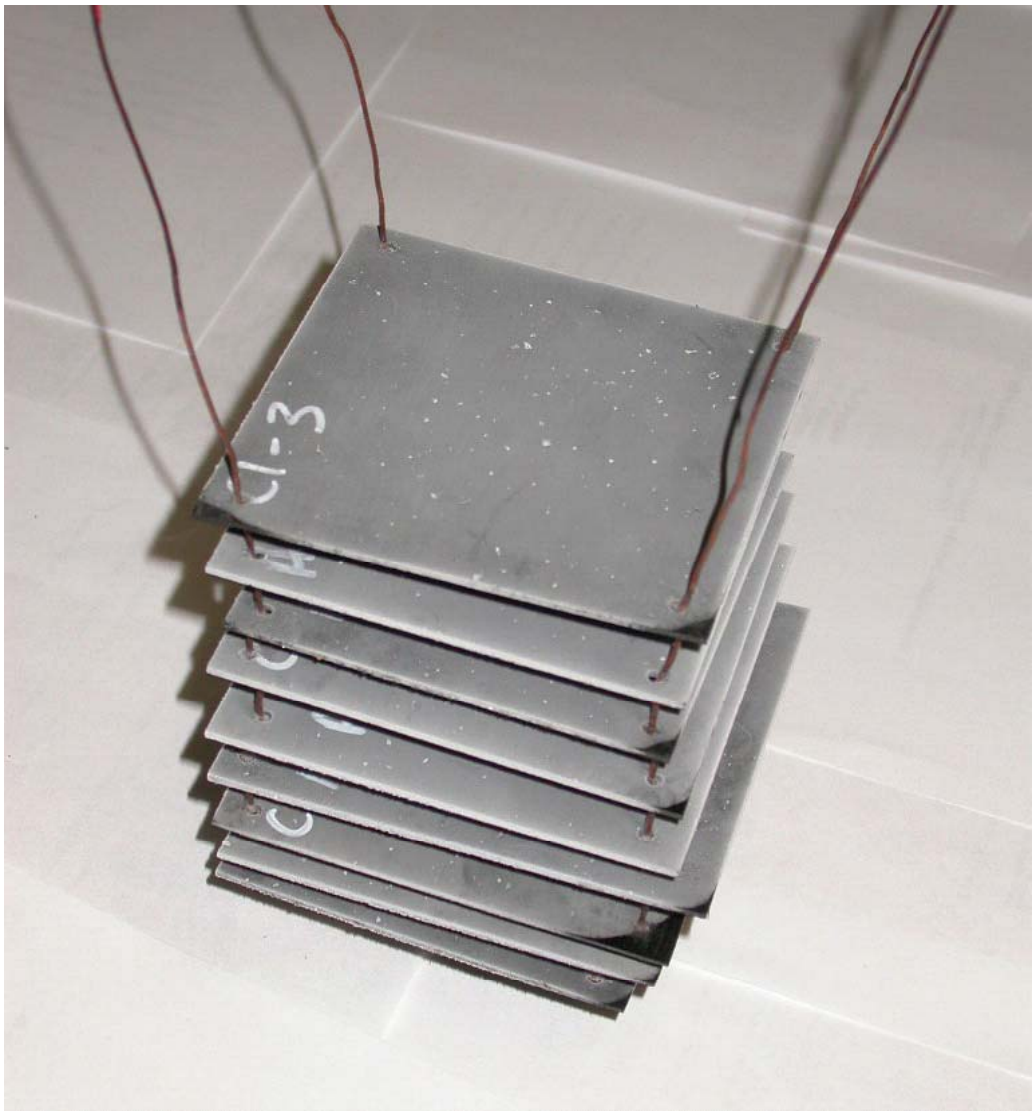

Figure 4.2.12 Frozen Specimens

After the specimens have been held at room temperature for 20 minutes, they are suspended in an oven at 127°C (260°F) to simulate the environment of the tanks and lines

when the fuel has been depleted and the space shuttle is reentering the atmosphere and heating up. The following figure shows the stack of specimens suspended in the oven.

Figure 4.2.13 Specimen Stack Hanging in Oven

After the specimens have been subjected to elevated temperatures for 20 minutes, the stack is removed and is held at room temperature for 20 minutes. Previous research found that polymers reach their maximum damage densities quickly when thermally cycled, so it was determined that 5 cycles would be sufficient to achieve the maximum level of damage that would occur. Therefore, the above described thermal cycle (LN_2, roomT, oven, roomT) is repeated 5 times and then the stack is dismantled. The specimens are then inspected for visual damage and the results recorded.

4.2.4 Drop-weight Impact Machine

The reusable launch vehicle's fuel tanks and fuel lines are vulnerable to low-velocity impacts which may cause enough damage to the material to cause permeation. For this reason, it was necessary to determine if the addition of a barrier layer would allow the composite to withstand a greater amount of impact before leaking.

In order to simulate an impact like that which is due to a dropped tool or inadvertent bumping, a Dynatup 8250 drop-weight impact apparatus was used. The impact equipment is displayed in Figure 4.2.14. Figure 4.2.15 displays the specimen placed in the impact.

Figure 4.2.14 Dynatup 8250 Impact Apparatus

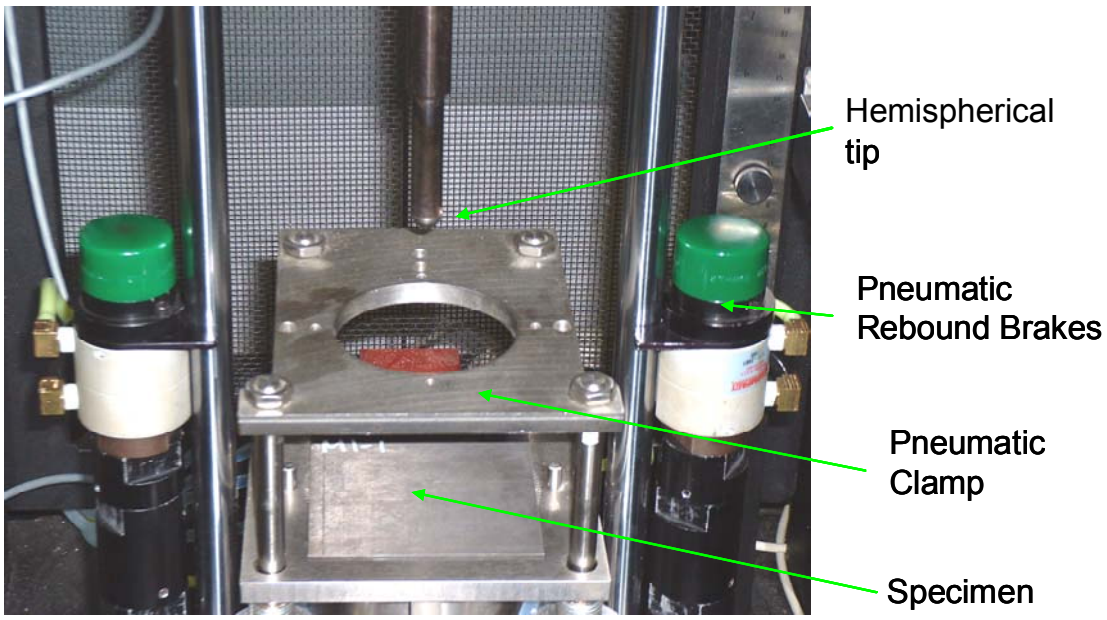

Figure 4.2.15 Dynatup 8250 Impact area

A half-inch diameter hemispherical tup had previously been found to provide a high level of matrix damage without penetrating the composite, so this was used in the Dynatup 8250 for all impacts. The tup is connected to a load cell and computer data acquisition system where the software will calculate such values as the impact energy, energy absorbed by the composite, velocity at impact, maximum impact load, and maximum deflection.

The Dynatup 8250 has a set of weights ranging from 23.4 N (5.27 lb) to 222 N (50 lb) which can be attached to the dropping mechanism in order to provide the desired impact energies. For this research, the lightest weight available for the test machine was used. The total weight of the dropping mechanism is 36.0 N (8.10 lb), which calculated by summing the weight of the attached weight and the weight of the tup. A sensor which

slides vertically along guide polls can be manually placed so that the impact occurs from the desired height, therefore resulting in the desired impact energy.

When the dropping mechanism is released, a flag attached to its side passes through a laser sensor just as the specimen is impacted. This sensor allows for the velocity of the impact to be calculated and also signals the pneumatic rebound brakes to fire when appropriate. The pneumatic rebound breaks are designed to fire when the flag reenters the velocity sensor in order to prevent the impactor from repeatedly impacting the specimen.

The Dynatup 8250 determines the velocity of the impactor, by using the following equation

$$V = w_{flag}/t_{flag}+g*(t_{imp}) \quad (1)$$

In the above equation w_{flag} is the width of the spacing between the leading edge of the velocity flag and the second leading edge (1 cm), t_{flag} is the time taken between the flags leading edge and second leading edge clearing the sensor, and t_{imp} is the time between the second leading edge clearing the sensor and the point just before impact initiation. The Dynatup software determines the energy at impact using the following equation where m is the mass dropping mechanism, and V is the velocity of the dropping mechanism.

$$I.E. = ½*m*V^2 \quad (2)$$

The Dynatup software determines the energy absorbed by the specimen, E_a, from the rebound velocity of the crosshead and tup, V_r, which was determined in the same way as the initial velocity. The equation for energy absorbed is displayed in the following equation.

$$E_a = \frac{1}{2} * m * [V - V_r]^2 \quad (3)$$

Before impacting any specimens, the sliding sensor is adjusted so that the dropping mechanism releases from the desired height. Next, velocity tests are run in order to ensure that the software is calculating consistent velocities and that the rebound brakes are firing consistently. Once it is determined that the software and hardware are behaving appropriately, the specimen is centered in the pneumatic clamp over the 3" (7.62 cm) diameter opening. This opening allows the specimen to deflect upon impact. Next, the pneumatic clamp is fully lowered onto the specimen and the dropping mechanism is released. As soon as the specimen has been impacted, as the flag reenters the laser sensor, the pneumatic rebound brakes are engaged in order to prevent the impactor from repeatedly impacting the specimen.

In order to determine if the addition of a barrier layer within the composite would increase the amount of impact it could withstand without leaking, the critical impact energy (CIE) if each type of hybrid and control was found. The critical impact energy is defined as the most amount of impact the specimen can withstand before leaking. Initially, a rough estimate of this value is determined by repeatedly impacting a single specimen. After each impact, the specimen is leak tested. The specimen is then subjected to a series of sequentially higher impacts until it begins to leak. Usually, the height of the impactor was adjusted in ½ " increments. At this point, the CIE estimate is narrowed down by impacting a fresh specimen at the energy which had caused the multiple impact specimen to leak, and then adjusting the impact for the following specimen. It is in this manner that an impact energy value is found at which the

specimens do not leak, but above which they do. This critical impact energy will be determined for both control and hybrid composites to determine if the addition of the barrier layer increases the energy that the composite can withstand before leaking.

CHAPTER 5 RESULTS AND DISCUSSION

This chapter will describe the results obtained from each step of the analysis and testing. The results described will follow the same order as the procedure itself: manufacture hybrids and controls, leak test all specimens, thermal cycle samples of each type of specimen, leak test the thermally cycled specimens, critical impact energy for all types of specimens (including those that had previously been thermal cycled), thermal cycle then leak test those specimens which had previously been impacted at the CIE. Table 5.1 displays the test matrix used for this experiment:

Table 5.1 Experimental Test Matrix

Test	Type of Hybrid						
	Control	Al foil (thin)	Al foil (thick)	Al Mylar® (thin)	Al Mylar® (thick)	β-Ti (no resin)	β-Ti (resin)
Manufacture	36	12	12	24	12	12	12
Leak test (after manufacture)	24	12	2	24	2	2	2
ΔT / Leak Test	3	3	2	3	2	2	2
Find CIE	29	12	5	15	7	11	11
ΔT (after impact) / Leak Test	2	2	**	2	**	**	**

5.1 Manufacture and Leak Test

5.1.1 Results

The following types of composite specimens were successfully manufactured: controls, aluminized Mylar® hybrids, aluminum foil hybrids, β-Ti (no resin/NASA) hybrids, β-Ti (resin/Boeing) hybrids.

Table 5.1.1 Successfully Manufactured Specimens

Type of Composite	# Specimens
Control	36
Aluminized Mylar® hybrids (t=6μm)	24
Aluminized Mylar® hybrids (t=50μm)	12
Aluminum foil hybrids (t=16μm)	12
Aluminum foil hybrids (t=35μm)	12
β-Ti (no resin/NASA) hybrids (t=152μm)	12
β-Ti (resin/Boeing) hybrids (t=127μm)	12

As described earlier in Section 4.3.1 Autoclave, each panel cured in the autoclave was then cut into 12 specimens. Specimens cut from the same panel ranged in thickness from .9mm to 1.15 mm. The following figure shows an example of a specimen from panel C1 in position 10 in the panel.

Figure 5.1.1 Graphite/Epoxy Composite Laminate Specimen

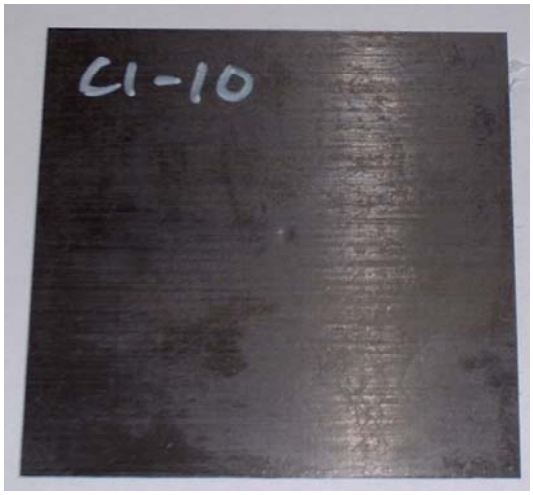

Three control panels were manufactured and labeled C1, C2, and C3. Two thin (6μm) Aluminized Mylar® hybrid panels were manufactured and labeled M1 and M2. One thick (50μm) Aluminized Mylar® hybrid panel was manufactured and labeled M3. One thin (16μm) Aluminum foil hybrid was manufactured and labeled A5 and one thick (35μm) Aluminum foil hybrid was manufactured and labeled A6. One β-Ti (no resin/NASA) hybrid panel was manufactured and labeled T1 and a β-Ti (resin/Boeing) hybrid panel was manufactured and labeled T2.

5.1.2 Discussion

Every specimen from panels C1, C2, A5, M1 and M2 was leak tested after manufacture and found to be leak free. For this reason, it was determined that it was not necessary to leak test every specimen from panels C3, A6, M3, T1 and T2. Leak testing 2 specimens from each panel was determined to be a sufficient sample from the panel to

conclude if it had been properly manufactured. Even if a specimen was leaking after manufacture but had not been leak tested, upon trying to determine the CIE, it would be clear if the specimen was leaking due to thermally induced stresses or due to impact(s). The reason for this, is that the leaking caused by impacts originates from the site of impact, while leaking caused by matrix cracking would occur through the entire surface.

5.2 Leak Test After Thermal Cycling

Due to the large difference in CTE between the matrix, fibers, and barrier layers, the stresses developed due to thermal cycling are of utmost concern. For this reason, a viable hybrid composite candidate must be able to withstand thermal cycling without delaminating and without becoming permeable to the cryogenic fuel. Each type of hybrid manufactured, as well as control specimens, was put through five thermal cycles to simulate the cryogenic temperature of the fuel and the elevated temperature of the tanks upon reentry to the atmosphere.

5.2.1 Results

After the thermal cycling, each of the specimens was subjected to a leak test with pressurized Helium gas, up to 30 psi, to determine if the thermal cycling had caused enough damage within the composite to cause it to leak. All hybrid composites as well as the control composites were found to be leak free after thermal cycling.

5.2.2 Discussion

As previously described, when preparing the specimens for thermal cycling, holes were drilled in the corners of each specimen so that they could be strung together with thermocouple wire and submerged in LN_2 and suspended in the oven. It was observed that all aluminized Mylar® hybrids and the β-Ti (no resin/NASA) hybrids delaminated at the corners after the holes were drilled. The following three figures show various magnifications of the delamination of an aluminized Mylar® hybrid taken using a stereoscope. The Figure 5.2.1 displays a magnification of the laminate from which one can observe the lay-up of the composite. In this case, the light layers are the 0 degree plies with the fibers running from left to right, while the dark layers are the 90 degree plies, where the fibers are coming in and out of the page.

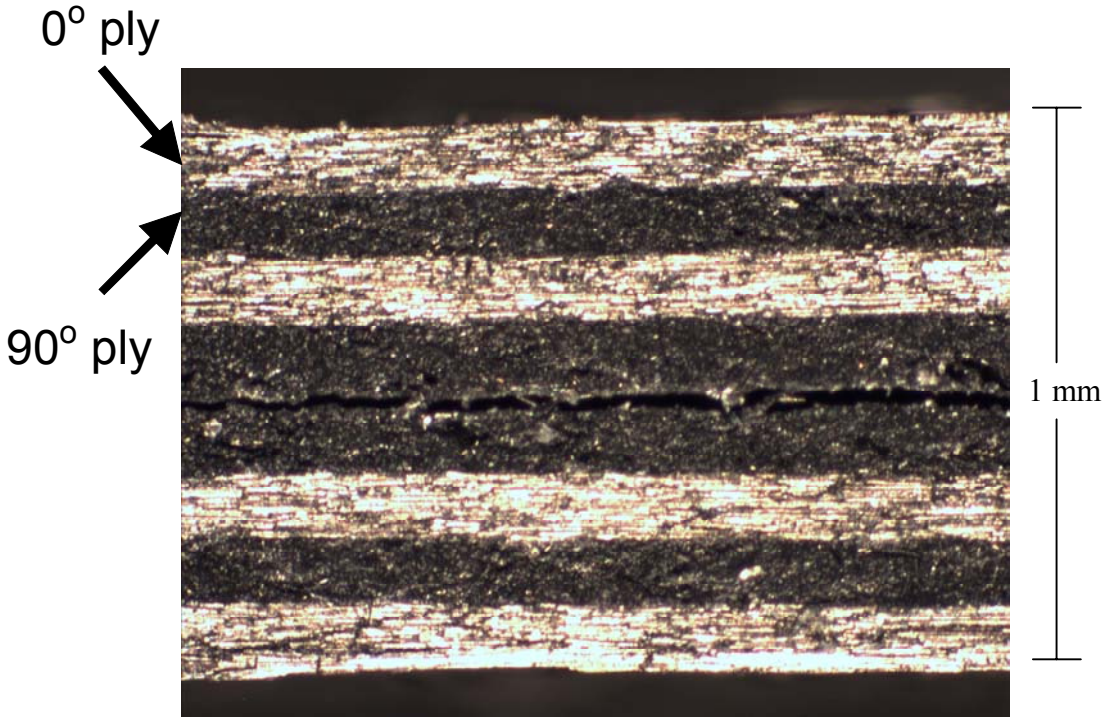

Figure 5.2.1 Aluminized Mylar® Hybrid Lay-Up

From Figure 5.2.2 it can be seen that the delaminations of the corners upon drilling could extend into the laminate as far as 6.5 mm.

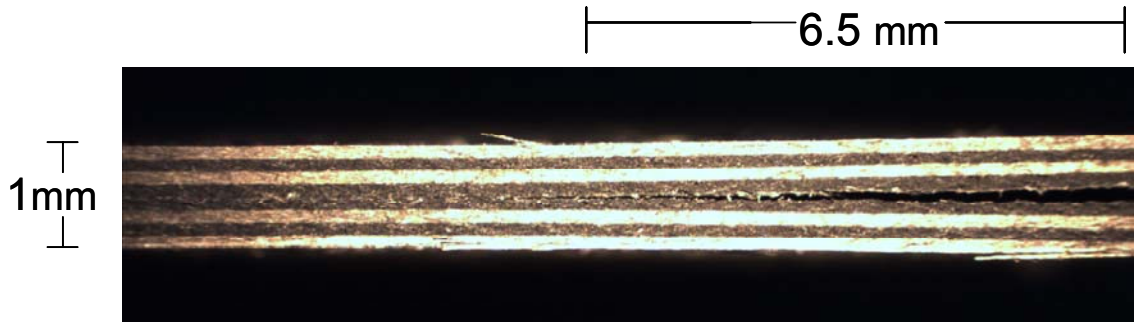

Figure 5.2.2 Aluminized Mylar® Hybrid Delamination

Figure 5.2.3 displays how the delaminations due to drilling could cause the corners to delaminate and open as much as 0.5 mm.

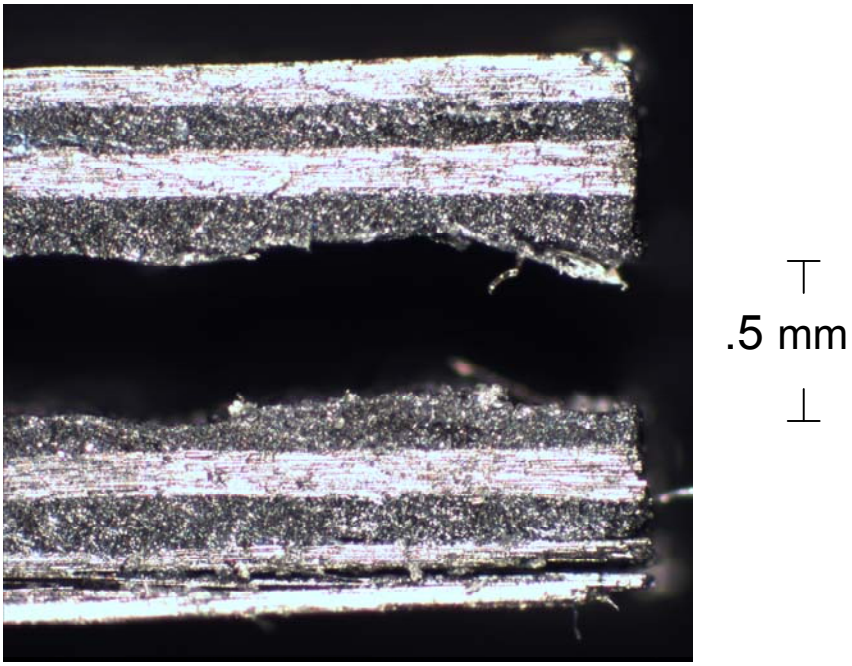

Figure 5.2.3 Aluminized Mylar® Hybrid Corner Delamination

Even though the aluminized Mylar® hybrids and the β-Ti (no resin/NASA) hybrids exhibited marginal adhesion to the composite, all types of hybrid composites, including the control specimens remained leak free after thermal cycling. Also, no visual damage due to thermal cycling was observed on any of the specimens. In theory, even if the thermal stresses are substantial enough to cause matrix microcracking, the barrier layer material will remain ductile enough to resist cracking and remain impermeable. These results indicate that embedding a barrier layer within a graphite epoxy composite may allow the laminates to withstand extreme thermal cycling while remaining leak free.

5.3 Critical Impact Energy

The cryotanks are vulnerable to low-velocity impacts which have the potential to damage the composite and lead to fuel permeation. For this reason, it is important to develop composites capable of withstanding impacts while retaining their impermeability. One goal of this research is to determine if the addition of the barrier within the graphite/epoxy composite would allow the composite to withstand greater impacts. Therefore, drop weight impact tests were used to determine the critical impact energy of each type of hybrid composite, as well as the control composites. The CIE is defined as the maximum amount of impact energy the composite can withstand while remaining leak free.

5.3.1 Results

Depending on the severity of the impact, various types of visual damage could be observed. In general, the more severe the visible damage, the more likely the composite was to leak, but this was not always the case. There were instances where very little damage was visible, but the composite specimen would leak. Conversely, there were instances when the impact damage appeared very severe, but the composite still remained impermeable.

In general, the first sign of visible damage was a small dent on the surface of the specimen, correlating to the site of impact, at this point there may be a slight oblong protrusion on the underside of the specimen, directly opposite the site of impact. Upon impacting with higher energy, usually one crack would appear around the site of impact, and the bottom surface would look slightly more severe and more oblong, at times slight

fiber delaminations could be observed. Impacting with even higher energies would cause a bigger dent at the site of impact, and almost always cause one to two cracks around the dent. The damage on the underside of the specimen would look very severe, extremely oblong, with obvious delaminations and fiber rupture directly beneath the site of impact.

The cracks observed on the surface of the impacted specimen always formed perpendicular to the direction of the fibers and started at the edge of the dent formed by the impact. The following two figures show the types of crack that can develop on the surface due to impacts. The black circles represent the dent formed by the impact, which is hard to distinguish from these pictures. At times, only one crack would form, and with increased impact energy, two cracks would form on each side of the dent, sometimes directly opposite from each other, and other times offset from each other. The offset cracks were observed much less frequently than the parallel cracks.

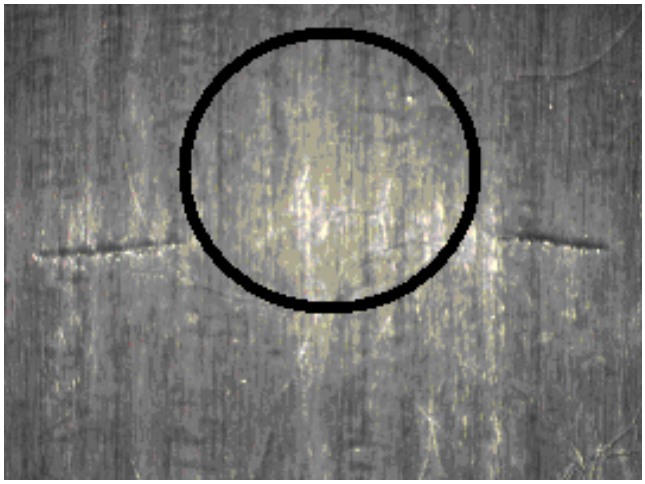

Figure 5.3.1 Parallel Surface Cracks Due to Impacting

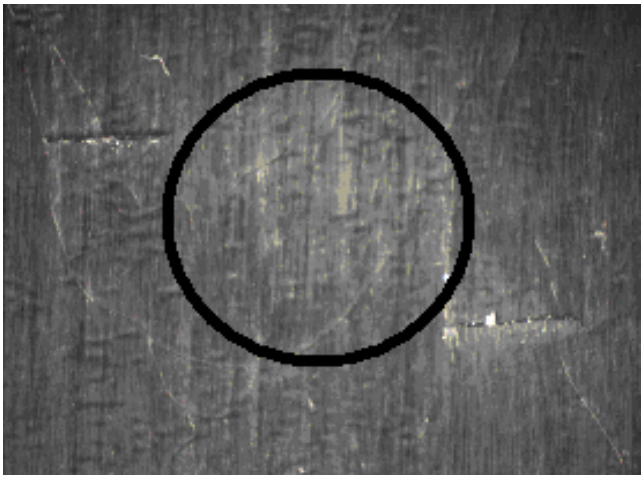

Figure 5.3.2 Offset Surface Cracks Due to Impacting

Initially, the CIE of the control composites was determined in order to quantify the amount of improvement that each type of barrier layer may provide to the impact resistance of the composite. Tables 5.3.1 – 5.3.3 display the results of the impact testing on each of the three control panel specimens which was performed in order to determine the critical impact energy value for the control composites.

Table 5.3.1 Impact Data from Control Specimens (Panel C1)

Specimen Name	Impact Energy J (ft-lb)	Impact Velocity m/s (ft/sec)	Maximum Load N (lb)	Leak Results
C1-1A	2.14 (1.58)	1.08 (3.54)	1072 (241)	no leak
C1-1B	3.09 (2.28)	1.30 (4.26)	1466 (330)	@ 69kPa (10 psi)
C1-2A	3.55 (2.62)	1.39 (4.57)	1947 (438)	no leak
C1-2B	4.01 (2.96)	1.48 (4.85)	1854 (417)	no leak
C1-2C	4.51 (3.33)	1.57 (5.14)	1987 (447)	no leak
C1-2D	5.19 (3.83)	1.68 (5.52)	2106 (473)	@ 138kPa (20 psi)
C1-4A	5.19 (3.83)	1.68 (5.52)	2075 (467)	@ 69kPa (10 psi)
C1-5A	4.80 (3.54)	1.62 (5.30)	1846 (415)	@ < 34kPa (5 psi)
C1-7A	4.28 (3.16)	1.53 (5.01)	1634 (367)	@ 207kPa (30 psi)
C1-8A	3.78 (2.79)	1.43 (4.70)	1628 (366)	no leak
C1-10A	3.82 (2.82)	1.44 (4.73)	1609 (362)	@ 172kPa (25 psi)
A1-11A	3.27 (2.41)	1.33 (4.37)	1443 (324)	no leak
C1-12A	3.21 (2.37)	1.32 (4.34)	1478 (332)	no leak

Table 5.3.2 Impact Data from Control Specimens (Panel C2)

Specimen Name	Impact Energy J (ft-lb)	Impact Velocity m/s (ft/sec)	Maximum Load N (lb)	Leak Results
C2-1A	3.71 (2.74)	1.42 (4.67)	1646 (370)	@ < 103kPa (15 psi)
C2-2A	3.27 (2.41)	1.34 (4.38)	1459 (328)	@ 172kPa (25 psi)
C2-4A	2.73 (2.01)	1.22 (4.00)	1316 (296)	no leak
C2-5A	2.68 (1.98)	1.21 (3.97)	1270 (285)	@ 138kPa (20 psi)
C2-7A	2.28 (1.68)	1.11 (3.65)	1089 (245)	no leak
C2-8A	2.22 (1.64)	1.10 (3.60)	1108 (249)	no leak

Table 5.3.3 Impact Data from Control Specimens (Panel C3)

Specimen Name	Impact Energy J (ft-lb)	Impact Velocity m/s (ft/sec)	Maximum Load N (lb)	Leak Results
C3-3A	4.26 (3.14)	1.52 (4.99)	1749 (393)	no leak
C3-3B	4.95 (3.65)	1.64 (5.38)	1864 (419)	no leak
C3-3C	5.97 (4.4)	1.80 (5.91)	2163 (486)	no leak
C3-3D	6.75 (4.98)	1.92 (6.29)	2374 (534)	no leak
C3-4A	6.06 (4.47)	1.82 (5.96)	2181 (490)	@ < 34kPa (5 psi)
C3-5A	5.34 (3.94)	1.71 (5.60)	1861 (418)	@ 138kPa (20 psi)
C3-6A	4.35 (3.21)	1.54 (5.05)	1701 (382)	no leak
C3-7A	4.32 (3.19)	1.53 (5.03)	1678 (377)	no leak
C3-8A	4.97 (3.67)	1.65 (5.40)	1900 (427)	@ < 34kPa (5 psi)
C3-9A	4.37 (3.22)	1.54 (5.06)	1845 (415)	@ 138kPa (20 psi)
C3-10A	3.86 (2.85)	1.45 (4.76)	1629 (366)	no leak
C3-11A	3.81 (2.81)	1.44 (4.73)	1640 (369)	@ 207kPa (30 psi)
C3-12A	3.39 (2.50)	1.36 (4.45)	1534 (345)	no leak

From the results of the drop weight impact tests performed on the control composites, it was found that control panel C1 exhibited a CIE of 2.52 ft-lb, control panel C2 exhibited a CIE of 1.78 ft-lb, and control panel C3 exhibited a CIE of 2.68. It is currently unknown why the variation in CIE occurred between the control panels, but to be conservative, from here on out, the CIE of panel C2 will be used when describing improvement factor seen with the various types of hybrid composites.

After the CIE of the control composites was determined, it was important to determine the CIE of each subsequent type of hybrid in order to determine if the addition of the barrier layer allowed for an increase in critical impact energy. Tables 5.3.4 – 5.3.6 display the drop weight impact test results for the Aluminized Mylar® hybrid specimens.

Table 5.3.4 Impact Data from Aluminized Mylar® Hybrid Specimens (Panel M1)

Specimen Name	Impact Energy J (ft-lb)	Impact Velocity m/s (ft/sec)	Maximum Load N (lb)	Leak Results
M1-1A	6.24 (4.60)	1.84 (6.04)	2264 (509)	no leak
M1-2A	6.82 (5.03)	1.93 (6.33)	2357 (530)	no leak
M1-4A	7.39 (5.45)	2.01 (6.58)	2420 (544)	no leak
M1-5A	7.80 (5.75)	2.06 (6.76)	2309 (519)	@ < 34kPa (5 psi)
M1-7A	7.06 (5.21)	1.96 (6.43)	2282 (513)	@ < 34kPa (5 psi)
M1-8A	6.66 (4.91)	1.91 (6.25)	2238 (503)	no leak

Table 5.3.5 Impact Data from Aluminized Mylar® Hybrid Specimens (Panel M2)

Specimen Name	Impact Energy J (ft-lb)	Impact Velocity m/s (ft/sec)	Maximum Load N (lb)	Leak Results
M2-1A	3.95 (2.92)	1.47 (4.82)	1557 (350)	no leak
M2-1B	4.69 (3.46)	1.60 (5.25)	1944 (437)	no leak
M2-1C	5.21 (3.85)	1.68 (5.51)	2011 (452)	no leak
M2-1D	6.11 (4.51)	1.83 (6.00)	2411 (542)	no leak
M2-2A	6.16 (4.54)	1.83 (6.00)	2171 (488)	no leak
M2-2B	6.83 (5.04)	1.93 (6.33)	2446 (550)	@ < 34kPa (5 psi)
M2-4A	6.26 (4.62)	1.85 (6.07)	2162 (486)	no leak
M2-5A	6.67 (4.92)	1.91 (6.27)	2290 (515)	no leak
M2-7A	6.86 (5.06)	1.93 (6.33)	2041 (459)	@ < 34kPa (5 psi)
M2-8A	6.56 (4.84)	1.89 (6.20)	2241 (504)	no leak

Table 5.3.6 Impact Data from Aluminized Mylar® Hybrid Specimens (Panel M3)

Specimen Name	Impact Energy J (ft-lb)	Impact Velocity m/s (ft/sec)	Maximum Load N (lb)	Leak Results
M3-1A	5.99 (4.42)	1.81 (5.93)	2142 (482)	no leak
M3-2A	6.98 (5.15)	1.95 (6.39)	2319 (521)	@ 207kPa (30 psi)
M3-3A	6.70 (4.94)	1.91 (6.27)	2390 (537)	no leak
M3-4A	6.66 (4.91)	1.90 (6.24)	2188 (492)	no leak
M3-5A	7.17 (5.29)	1.98 (6.48)	2387 (537)	no leak

From the results of the drop weight impact tests performed on the Aluminized Mylar® hybrid composites, it was found that the two panels containing the thinnest layer of Mylar® exhibited similar critical impact energies of 4.97 ft-lb and 4.79 ft-lb for panels M1 and M2 respectively. Panel M3, containing the thicker layer of Mylar® exhibited a CIE of 4.93 ft-lb. The CIE for these Mylar® hybrids represents an improvement factor over the CIE of the control specimens of 2.8, 2.7, 2.77 for panels M1, M2, and M3 respectively.

Tables 5.3.7 – 5.3.9 and display the results of the drop weight impact tests performed on the specimens from 3 panels of Aluminum foil hybrids. Panel A1 and A5 contain the thin layer of Aluminum foil, while panel A6 contains the thicker layer of foil. Panel A1 was not earlier included in the list of successfully manufactured composite panels. This is because, due to a malfunction with the autoclave during the cure of this panel, the cure had to be stopped mid-cycle. For this reason, it was determined that this panel would not be a good comparison to those panels who received the proper cure cycle. But, in the interest of investigating the effects of stopping a panel mid-cure, this panel was subjected to drop weight impact tests along with the other panels.

Table 5.3.7 Impact Data from Aluminum Foil Hybrid Specimens (Panel A1)

Specimen Name	Impact Energy J (ft-lb)	Impact Velocity m/s (ft/sec)	Maximum Load N (lb)	Leak Results
A1-EA	4.99 (3.68)	1.65 (5.41)	1607 (361)	@ 138kPa (20 psi)
A1-FA	4.51 (3.33)	1.57 (5.15)	1628 (366)	no leak
A1-GA	4.49 (3.31)	1.56 (5.13)	1630 (366)	no leak
A1-HA	5.02 (3.70)	1.65 (5.42)	1635 (368)	@ 172kPa (25 psi)
A1-IA	3.70 (2.73)	1.42 (4.65)	1728 (388)	no leak
A1-JA	5.46 (4.03)	1.73 (5.66)	1707 (384)	@ 69kPa (10 psi)
A1-KA	5.86 (4.32)	1.79 (5.86)	1630 (367)	@ < 34kPa (5 psi)
A1-LA	5.45 (4.02)	1.72 (5.65)	1629 (366)	no leak

Table 5.3.8 Impact Data from Aluminum Foil Hybrid Specimens (Panel A5)

Specimen Name	Impact Energy J (ft-lb)	Impact Velocity m/s (ft/sec)	Maximum Load N (lb)	Leak Results
A5-1A	4.05 (2.99)	1.48 (4.87)	1744 (392)	no leak
A5-1B	4.62 (3.41)	1.58 (5.20)	2041 (459)	no leak
A5-1C	5.02 (3.70)	1.65 (5.42)	2330 (524)	no leak
A5-1D	5.57 (4.11)	1.74 (5.72)	2282 (513)	no leak
A5-1E	6.00 (4.43)	1.81 (5.93)	2348 (528)	no leak
A5-1F	6.51 (4.80)	1.88 (6.17)	2580 (580)	no leak
A5-1G	6.82 (5.03)	1.93 (6.32)	2628 (591)	no leak
A5-1H	7.27 (5.36)	1.99 (6.52)	2583 (581)	@ 7kPa (1 psi)
A5-2A	7.25 (5.35)	1.99 (6.52)	2520 (566)	@ 69kPa (10 psi)
A5-4A	6.78 (5.00)	1.92 (6.30)	2383 (536)	no leak
A5-5A	6.78 (5.00)	1.92 (6.30)	2249 (506)	@ < 34kPa (5 psi)
A5-7A	6.26 (4.62)	1.85 (6.06)	2146 (483)	@ 138kPa (20 psi)
A5-8A	5.81 (4.29)	1.78 (5.84)	2081 (468)	@ 138kPa (20 psi)
A5-10A	4.92 (3.63)	1.64 (5.37)	1905 (428)	@ 34kPa (5 psi)
A5-11A	4.39 (3.24)	1.55 (5.07)	1814 (408)	no leak
A5-12A	4.38 (3.23)	1.55 (5.07)	1808 (407)	no leak

Table 5.3.9 Impact Data from Aluminum Foil Hybrid Specimens (Panel A6)

Specimen Name	Impact Energy J (ft-lb)	Impact Velocity m/s (ft/sec)	Maximum Load N (lb)	Leak Results
A6-1A	5.27 (3.89)	1.69 (5.56)	2056 (462)	no leak
A6-2A	5.88 (4.34)	1.79 (5.87)	2140 (481)	@ 207kPa (30 psi)
A6-3A	5.52 (4.07)	1.73 (5.69)	2057 (463)	@ 207kPa (30 psi)
A6-4A	5.12 (3.78)	1.67 (5.48)	2016 (453)	no leak
A6-5A	5.04 (3.72)	1.66 (5.44)	1975 (444)	no leak

From the results of the drop weight impact testing of the Aluminum foil hybrid composites, it was found that the two panels containing the thin layer of Aluminum foil exhibited CIEs of 3.32 ft-lb, and 3.24 ft-lb for panels A1 and A5 respectively. Panel A6, containing the thicker Aluminum foil, was found to have a CIE of 3.84 ft-lb. The CIE for these Aluminum foil hybrids represents an improvement factor over the CIE of the control specimens of 1.87, 1.82, and 2.16 for panels A1, A5, and A6 respectively.

Table 5.3.10 and Table 5.3.11 display the results of the drop weight impact tests performed on the β-Ti (no resin/NASA) hybrid panel T1 and the β-Ti (resin/Boeing) hybrid panel T2.

Table 5.3.10 Impact Data from β-Ti (no resin/NASA) Hybrid Specimens (Panel T1)

Specimen Name	Impact Energy J (ft-lb)	Impact Velocity m/s (ft/sec)	Maximum Load N (lb)	Leak Results
T1-1A	7.24 (5.34)	1.98 (6.51)	2676 (602)	no leak
T1-1B	7.96 (5.87)	2.08 (6.83)	2758 (620)	@ 69kPa (10 psi)
T1-2A	7.92 (5.84)	2.08 (6.81)	2621 (589)	@ 69kPa (10 psi)
T1-3A	7.58 (5.59)	2.03 (6.66)	2692 (605)	@ 69kPa (10 psi)
T1-4A	7.12 (5.25)	1.97 (6.46)	2560 (576)	@ 69kPa (10 psi)
T1-5A	6.62 (4.88)	1.90 (6.23)	2399 (539)	@ 103kPa (15 psi)
T1-7A	6.17 (4.55)	1.83 (6.01)	2267 (510)	@ 103kPa (15 psi)
T1-8A	5.82 (4.29)	1.78 (5.84)	2259 (508)	@ 207kPa (30 psi)
T1-10A	5.53 (4.08)	1.74 (5.70)	2322 (522)	no leak
T1-11A	5.53 (4.08)	1.73 (5.69)	2319 (521)	no leak

Table 5.3.11 Impact Data from β-Ti (resin/Boeing) Hybrid Specimens (Panel T2)

Specimen Name	Impact Energy J (ft-lb)	Impact Velocity m/s (ft/sec)	Maximum Load N (lb)	Leak Results
T2-1A	6.09 (4.49)	1.82 (5.97)	2495 (561)	no leak
T2-2A	6.68 (4.93)	1.91 (6.26)	2687 (604)	no leak
T2-3A	7.16 (5.28)	1.98 (6.48)	2808 (631)	no leak
T2-4A	7.97 (5.88)	2.08 (6.84)	2967 (667)	no leak
T2-5A	8.57 (6.32)	2.16 (7.08)	2970 (668)	no leak
T2-7A	9.61 (7.09)	2.29 (7.51)	3097 (696)	@ < 34kPa (5 psi)
T2-8A	8.82 (6.51)	2.19 (7.19)	3285 (739)	@ < 34kPa (5 psi)
T2-10A	7.92 (5.84)	2.08 (6.81)	2885 (649)	no leak
T2-11A	7.85 (5.79)	2.07 (6.78)	2993 (673)	no leak

From the results of the drop weight impact tests performed on the two samples of β-Titanium, it was found that the β-Ti (no resin/NASA) hybrid panel T1 exhibited a CIE of 4.08 ft-lb, and the β-Ti (resin/Boeing) hybrid panel T2 exhibited a CIE of 6.32 ft-lb.

The CIE for these β-Titanium foil hybrids represents an improvement factor over the CIE of the control specimens of 2.3 and 3.56 for panels T1 and T1 respectively.

5.3.2 Discussion

The results of these drop weight impact tests are very promising for the future of hybrid composites for use in applications where retaining impermeability after low-velocity impacts is crucial. All types of hybrid exhibited an increase in critical impact energy needed to cause the composite to leak. Depending on the type of barrier layer material, the CIE of the composite was improved by varying amounts. Table 5.3.12 displays the results for the critical impact energy for all control panels and hybrid panels.

Table 5.3.12 Critical Impact Energy and Improvement Factor over Control

Specimen Type (Panel , # tested)	Critical Impact Energy J (ft-lb)	Improvement Factor
Control (C1 , 9)	3.42 (2.52)	n/a
Control (C2 , 6)	2.41 (1.78)	n/a
Control (C3 , 11)	3.63 (2.68)	n/a
Al foil hybrid (A1 , 8)*	4.50 (3.32)	1.87
Al foil hybrid (A5 , 9)	4.39 (3.24)	1.82
Al foil hybrid (A6 , 5) - thick	5.20 (3.84)	2.16
Mylar® hybrid (M1 , 6)	6.73 (4.97)	2.80
Mylar® hybrid (M2 , 6)	6.49 (4.79)	2.70
Mylar® hybrid (M3 , 6) - thick	6.68 (4.93)	2.77
β-Titanium hybrid (T1 , 9) - no resin	5.53 (4.08)	2.30
β-Titanium hybrid (T2 , 9) - resin	8.27 (6.10)	3.43

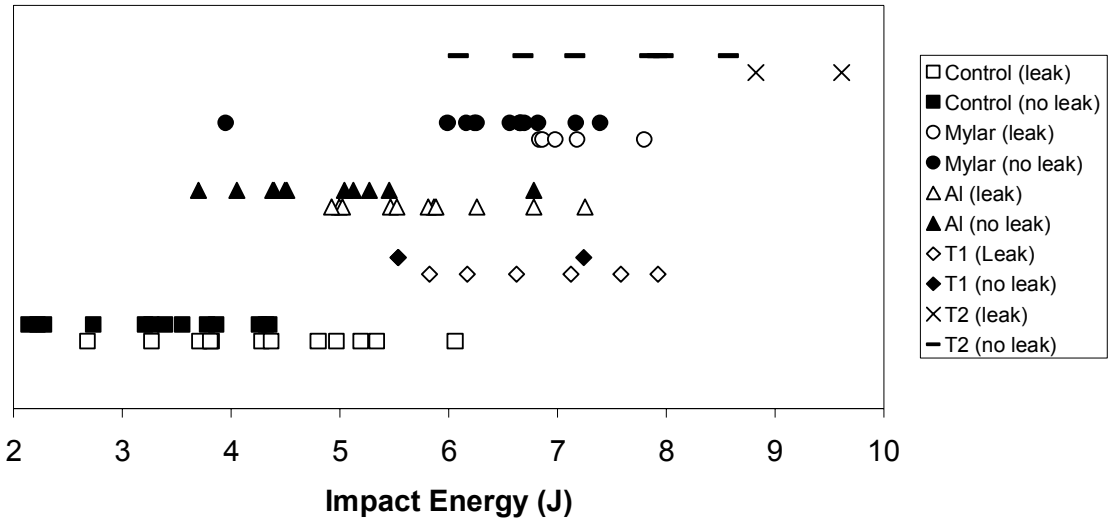

Figure 5.3.3 Distribution of Impacts for Hybrids and Controls

Figure 5.3.13 displays the distribution of impact energy sustained by each type of composite as well as whether or not the specimen leaked. It should be noted that there are some outlying points where a specimen withstood more impact energy without leaking than the majority of the other specimens of the same type. CIE data points, for non-leaking specimens, with higher than impacts than caused other similar specimens to leak were not included in calculating the critical impact energy of the type of composite. More specimens need to be subjected to impact and leak tests to narrow further down on the actual value of CIE. This will be discussed further in Chapter 7, Recommendations.

From these results it can be seen that the β-Titanium 15-3 (resin coated) hybrid exhibited the highest improvement in critical impact energy of the control. This is a substantial increase over the improvement of CIE of the other types of hybrid composites. Due to the ambiguity surrounding the properties of the various heat treatments of β-Titanium 15-3 compounded with the additional variability induced by the fact that one β-Titanium foil was resin coated while the other was not, it is difficult to determine the

exact cause for the difference in CIE exhibited by the two β-Titanium hybrids. It can be postulated that the reduced modulus of the Boeing/with resin β-Titanium 15-3 sample, caused by the solution treatment and rapid quenching, allows this material to behave in a tougher manner, able to withstand greater impacts and deformation, while still retaining its structural integrity, and most importantly for the purposes of this research, retaining its impermeability. It can also be postulated that the addition of the resin, coated on the surface of this titanium, allowed for a much higher titanium/composite adhesion which aided in the impact resistance of the composite.

The hybrid composites which performed next best in improving CIE of the control composites were the Mylar® hybrids. Surprisingly, these Mylar® hybrids outperformed the β-Titanium 15-3 (no resin coated) hybrids which performed on a comparable level to the thick Aluminum foil hybrid composites.

The fact that the Mylar® hybrids performed very well under impact is also not surprising. These thin foils are extremely ductile, and since, while embedded within the composite, they are constrained from extreme deformation due to the impacts, they are likely to retain their impermeability even if the composite itself was rendered permeable due to the impact. The same is true for the Aluminum foil hybrids, the aluminum foil material itself is less ductile than the Mylar®, which may be the reason for its poor performance in comparison.

As a whole, the drop weight impact tests proved very promising for the future of hybrid composites. Every type of barrier layer hybrid made a significant improvement on the amount of impact that the composites could withstand before leaking. Improving the

CIE of these composites is crucial for them to become a viable option for applications where they must withstand impacts and remain impermeable.

5.4 Critical Impact Energy After Thermal Cycling

Another important factor to investigate surrounding these hybrid composites for use on the cryogenic fuel tanks is how they will perform when subjected to multiple missions (multiple thermal cycles). It is proposed that damage caused by thermal cycling will cause the composites to have reduced impact resistance. It is important for these composites to withstand multiple missions (thermal cycles) as well as multiple impacts (before and after each mission). Therefore, drop weight impact tests were performed on specimens of each type that had previously been thermally cycled to determine if they exhibited a reduction in impact resistance. This section will discuss the results of the drop weight impact tests for the various types of composite specimens.

5.4.1 Results

Table 5.4.1 displays the results from the drop weight impact tests of the previously thermally cycled control specimens from panel C1. These specimens were found to exhibit a CIE of 2.42 ft-lb which translates to a 3.96% reduction in CIE as compared to specimens from the same panel which had not been previously thermally cycled.

Table 5.4.1 Impact Data from Thermally Cycled Control Composites (Panel C1)

Specimen Name	Impact Energy J (ft-lb)	Impact Velocity m/s (ft/sec)	Maximum Load N (lb)	Leak Results
C1-3A	3.25 (2.40)	1.33 (4.37)	1461 (328)	@ 69kPa (10 psi)
C1-3B	3.25 (2.40)	1.33 (4.36)	1473 (331)	no leaks
C1-6A	3.29 (2.43)	1.34 (4.39)	1454 (327)	no leaks
C1-9A	3.31 (2.44)	1.34 (4.40)	1477 (332)	no leaks

Table 5.4.2 and Table 5.4.3 display the results from the drop weight impact tests of the previously thermally cycled Aluminum foil hybrid specimens from panels A5 and A6. These specimens were found to exhibit CIEs of 3.22 ft-lb and 3.83 ft-lb which translates to a .46% and .13% reduction in CIE of specimens from panels A5 and A6 respectively, as compared to specimens from the same panel which had not been previously thermally cycled. This reduction in CIE is so small it should be considered negligible.

Table 5.4.2 Impact Data from Thermally Cycled Al Foil Hybrids (Panel A5)

Specimen Name	Impact Energy J (ft-lb)	Impact Velocity m/s (ft/sec)	Maximum Load N (lb)	Leak Results
A5-3A	4.38 (3.23)	1.55 (5.07)	1746 (392)	no leak
A5-6A	5.17 (3.81)	1.68 (5.50)	1890 (425)	@ 172kPa (25 psi)
A5-9A	4.35 (3.21)	1.54 (5.05)	1821 (409)	no leak

Table 5.4.3 Impact Data from Thermally Cycled Al Foil Hybrids (Panel A6)

Specimen Name	Impact Energy J (ft-lb)	Impact Velocity m/s (ft/sec)	Maximum Load N (lb)	Leak Results
A6-6A	5.19 (3.83)	1.68 (5.52)	2009 (452)	no leak

Table 5.4.4 and 5.4.5 display the results from the drop weight impact tests of the previously thermally cycled Mylar® specimens from panels M2 and M3. These specimens were found to exhibit CIEs of 4.67 ft-lb and 4.33 ft-lb which translates to a 2.57% and 12.08% reduction in CIE of specimens from panels M2 and M3 respectively, as compared to specimens from the same panel which had not been previously thermally cycled.

Table 5.4.4 Thermally Cycled M2

Specimen Name	Impact Energy J (ft-lb)	Impact Velocity m/s (ft/sec)	Maximum Load N (lb)	Leak Results
M2-3A	6.44 (4.75)	1.87 (6.14)	2204 (495)	no leak
M2-6A	6.94 (5.12)	1.94 (6.36)	2224 (500)	@ < 34kPa (5 psi)
M2-9A	6.22 (4.59)	1.84 (6.04)	2153 (484)	no leak

Table 5.4.5 Thermally Cycled M3

Specimen Name	Impact Energy J (ft-lb)	Impact Velocity m/s (ft/sec)	Maximum Load N (lb)	Leak Results
M3-6A	6.72 (4.96)	1.91 (6.28)	2083 (468)	@ 103kPa (15 psi)
M3-9A	5.87 (4.33)	1.79 (5.87)	2093 (471)	no leak

Table 5.4.6 and Table 5.4.7 display the results from the drop weight impact tests of the previously thermally cycled β-Titanium hybrid specimens from panels T1 and T2. These specimens were found to exhibit CIEs of 3.37 ft-lb and 5.11 ft-lb which translates

to a 17.4% and 16.23% reduction in CIE of specimens from panels T1 and T2 respectively, as compared to specimens from the same panel which had not been previously thermally cycled.

Table 5.4.6 Thermally Cycled T1

Specimen Name	Impact Energy J (ft-lb)	Impact Velocity m/s (ft/sec)	Maximum Load N (lb)	Leak Results
T1-6A	5.64 (4.16)	1.75 (5.75)	2065 (464)	@ 69kPa (10 psi)
T1-9A	4.57 (3.37)	1.58 (5.18)	2033 (457)	no leak

Table 5.4.7 Thermally Cycled T2

Specimen Name	Impact Energy J (ft-lb)	Impact Velocity m/s (ft/sec)	Maximum Load N (lb)	Leak Results
T2-6A	7.84 (5.78)	2.07 (6.78)	2922 (657)	@ < 34kPa (5 psi)
T2-9A	6.93 (5.11)	1.94 (6.37)	2794 (628)	no leak

5.4.2 Discussion

The results of the drop weight impact tests performed on previously thermally cycled specimens can lead to some generalized conclusions. It appears that, depending upon the type of composite, thermal cycling can range from having no effect on the subsequent impact resistance to having a significant reduction in impact resistance. Regardless, even after five extreme thermal cycles the specimens still exhibit an increase in CIE as compared to the control specimens, which is promising for these materials.

Table 5.4.8 displays the CIE of each type of specimen which had been previously thermally cycled. The table also displays the percent reduction in CIE from the value of the non-thermally cycled specimens from the same panel.

Table 5.4.8 Critical Impact Energies of Thermally Cycled Specimens

Specimen Type (Panel , # tested)	Critical Impact Energy (ft-lb)	% Reduction in CIE after ΔT	Improvement Factor
Control (C1 - after ΔT , 3)	2.42	3.96%	n/a
Al foil hybrid (A5 - after ΔT , 3)	3.22	0.46%	1.81
Al foil hybrid (A6 after ΔT , 3) - thick	3.83	0.13%	2.16
Mylar® hybrid (M2 after ΔT , 3)	4.67	2.57%	2.63
Mylar® hybrid (M3 after ΔT , 3) - thick	4.33	12.08%	2.44
β-Titanium hybrid (T1 after ΔT , 3) - no resin	3.37	17.40%	1.90
β-Titanium hybrid (T2 after ΔT , 3) - resin	5.11	16.23%	2.88

These results indicate a trend of reduction in CIE after thermal cycling, but more specimens need to be tested in order to confirm these results.

5.5 Thermal Cycling After Impact

Another important factor to investigate surrounding these hybrid composites for use on the cryogenic fuel tanks is how they will perform when subjected to multiple missions (multiple thermal cycles) and multiple impacts. In order for these materials to be a viable option for material for the LH_2 and LO_2 cryotanks, they must be able to withstand multiple missions (thermal cycles) as well as multiple impacts (before and after each mission). One concern is that the damage caused by an impact would be compounded with the damage caused by subsequent thermal cycling and then cause permeation. For this reason, it was important to investigate the effects of thermal cycling

specimens after they had been subjected to impacts at their CIE, but that were not yet leaking.

5.5.1 Results

For this experiment, two previously impacted specimens from each the Aluminized Mylar® hybrids, Aluminum foil hybrids, and control composites, were subjected to 5 thermal cycles. The specimens chosen for this test were those which had been previously impacted near the CIE, but without enough energy to cause permeation. The specimens chosen from each panel were: from panel M2, specimens 5 and 8, from panel A5, specimens 11 and 12, and from panel C1, specimens 11 and 12. The following table displays the specimen panel and number and the impact at which each was subjected before undergoing the thermal cycling as well as the previously determined CIE for the particular panel of specimens.

Figure 5.5.1 Impacted Specimens Subsequently Subjected to Thermal Cycling

Specimen #	Impact Energy	CIE of Panel
M2-5	4.92	4.79
M2-8	4.84	4.79
A5-11	3.24	3.24
A5-12	3.23	3.24
C1-11	2.41	2.52
C1-12	2.37	2.52

After thermally cycling each of these previously impacted specimens, each specimen was leak tested in order to determine if the combination of damage from the

impact and thermal cycling was enough to cause the specimen to leak. The results of these leak tests determined that all of the previously non-leaking specimens remained leak free after thermal cycling.

5.5.2 Discussion

The results from thermal cycling after impacting indicate that the damage from the impacts combined with the damage caused by thermal cycling was not enough to cause leaking in the specimens. This is a promising, result for the future of these hybrid composites and the control composites for applications where it is critical the material retains its impermeability even after impacts and thermal cycles.

These results indicate that even when the graphite/epoxy composite is impacted with almost enough energy to cause a leak, the damage incurred by subsequent thermal cycling will not cause the material to leak. The materials for use on the LH_2 and LO_2 cryogenic fuel tanks of NASA's RLVs will be expected to withstand several missions (thermal cycles) and there is a possibility of impacts occurring during maintenance in between missions, so these results are very promising for the future use of these materials in this extreme application. Due to the limited number of specimens available for this part of the experiment, these results may not be statistically significant. Further testing needs to be conducted confirm these results.

CHAPTER 6 SUMMARY AND CONCLUSIONS

The research described in this thesis investigated an approach for improving a graphite/epoxy's resistance to thermal stresses and low-velocity impacts. In order to reduce the weight of the next generation RLVs, NASA would like to use composites for their LH_2 and LO_2 cryogenic fuel tanks which are exposed to extreme changes in temperature and low velocity impacts, both of which can cause fuel permeation which can lead to catastrophic failure. The main objective of this research was to develop durable hybrid matrix composites able to withstand extreme thermal cycles and low velocity impacts while retaining their impermeability.

Specifically, this research attempted to determine if the addition of a barrier layer embedded within a graphite/epoxy composite during manufacture could:

- Increase the percent of composites which are leak free after manufacture
- Improve the critical impact energy needed to cause the composite to leak
- Allow the composites to withstand extreme thermal stresses and remain leak free

The baseline composite material was an IM7/977-2 composite laminate, which is the same material which was used in for the face sheets of the X-33's sandwich structure cryogenic fuel tanks. All hybrid composites as well as the control specimens were manufactured using an autoclave. The composites were leak tested using pressurized Helium gas and thermal cycled using LN2 to simulate the cryogenic temperatures of the fuel tank. Drop weight impact tests were performed to simulate a low-velocity impact which might occur due to dropped tools or inadvertent bumping.

Hybrid composites containing Aluminized Mylar®, Aluminum foil, and β-titanium were successfully manufactured along with control composites. Upon cure, once the epoxy cools below its T_g and the material "locks up", stresses begin to develop within the composite itself, and between the composite material and the barrier layer. These stresses could potentially cause damage to the composite material and the barrier layer which could cause the laminate to leak. After manufacture, all hybrid specimens, as well as the control specimens, were leak tested and found to be leak free. Previous research conducted on woven composite laminates indicated that it may be difficult to obtain an impermeable composite feedline without extreme care taken during manufacture. Permeability after manufacture was not even an issue for the non-woven $[0/90]_{2S}$ lay-up investigated for this research. The fact that the hybrid composites remained leak free after manufacture is very promising for the potential of these materials.

In order to simulate the thermal stresses experienced by the cryotanks on the RLVs, all hybrid and control specimens were thermal cycled 5 times. The actual usage temperatures of the cryotanks range from -253°C (20K), the temperature of the LH_2, to 127°C (400K), the elevated temperatures upon re-entry. For the purposes of this research LH_2 could not be used for safety reasons, so LN_2 was used instead. Each cycle consisted of 20 minutes immersed in LN_2 -196°C (77K), 20 at room temperature, 20 minutes at an elevated temperature 127°C (400K, 260°F) , and then 20 minutes at room temperature.

Due to the difference in coefficient of thermal expansion between the matrix, fibers, and barrier layer materials, large changes in temperature cause stresses to build up in the laminate. These thermal stresses can cause matrix microcracking which can lead to

fuel permeation. For this reason, after the specimens were subjected to thermal cycling, all hybrid and control specimens were leak tested using pressurized Helium to determine if the damage caused by thermal stresses was enough to allow permeation.

In preparing the specimens for thermal cycling, holes were drilled in each of the four corners of the specimens. Both the Aluminized Mylar® hybrid specimens and the β-titanium (no resin/NASA) hybrid exhibited slight delaminations at the corners after the holes were drilled. This suggests that the adhesion of the Mylar® and the β-titanium (no resin/NASA) layers to the composite itself was marginal. In order for these types of hybrid composites to be viable options for use in these extreme applications, the adhesion of the barrier layer to the composite must be improved. Possible solutions include using an adhesive material to bond the barrier layer to the composite, or use a pickling agent on the barrier layer to scratch the surface and make it more likely to retain a strong bond with the graphite/epoxy composite.

All hybrid and control specimens were found to be leak free after thermal cycling which promising for the future use of hybrid IM7/977-2 composites. The fact that these hybrid composites could withstand this extreme change in temperature without sustaining enough damage to cause the composite to leak to pressurized Helium gas and without delaminating, is very promising for the potential of hybrid composites for use in applications of even more extreme temperature ranges.

In order to simulate low-velocity impacts to which the fuel tanks and especially the feedlines may be exposed, drop weight impact tests were performed on all of the hybrid specimens and control specimens. Low-velocity impacts such as what might occur due to a dropped tool or inadvertent bumping can cause damage within the

composite which can lead to fuel permeation through the thickness of the laminate. For this reason, it was important to determine if the addition of the barrier layer materials would increase the amount of impact that the composites can withstand while remaining impermeable. Using drop weight impact tests, the critical impact energy of each type of hybrid and the controls was determined. This critical impact energy is defined as the most amount of impact that the composite can withstand without leaking.

The results of the impact tests indicate that all types of hybrids exhibit an increase in critical impact energy over the control specimens. Depending upon the type of barrier layer, the CIE was increased to various levels. The thin aluminum foil hybrids exhibited an increase in CIE of approximately 3.24 ft-lb which represents an improvement factor of 1.82 times that of the control. The thick aluminum foil hybrids exhibited an increase in CIE of approximately 3.84 ft-lb which represents an improvement factor of 2.16 times that of the control. The thin aluminized Mylar® hybrid panels exhibited an increase in CIE of approximately 4.79 ft-lb and 4.97 ft-lb which represents improvement factors of 2.7 and 2.8 times that of the control. The β-titanium (no resin/NASA) hybrids exhibited a CIE of 4.08 ft-lb which translates to an improvement of 2.3 times the control, while the β-titanium (resin/Boeing) hybrids exhibited a CIE of 6.32 ft-lb, which represents an improvement of 3.56 times that of the control.

From the results of the drop weight impact tests, it can be concluded that the β-titanium (resin/Boeing) hybrid composites far out performed the other types of hybrids with respect to critical impact energy. The actual mechanical properties of this film are not confirmed, but work is underway by Mathew Hammond to characterize the effects of various heat treatments on the mechanical properties of β-titanium 15-3. Preliminary

results from his testing suggest that β-titanium 15-3 which has been solution treated at 788°C (1450°F) and rapid argon quenched will have a reduction in modulus as compared with the as received β-titanium and other heat treatments. Reducing the modulus increases the toughness of the material, which could be a reason that this material far outperformed the other interleaf materials. The thicker aluminum foil and Mylar® hybrids exhibited CIEs similar to their thinner interleaf hybrid counterparts. The reduction in impact resistance which can accompany an increase in interleaf thickness may have been cancelled out by the increase in mechanical properties associated with thicker films of these materials.

Results from impacting after thermal cycling suggest that damage caused by thermal cycling tends to reduce the CIE of the composite, but further testing needs to be conducted in this area. Results from thermal cycling after impacting suggest that the damage due to the thermal cycling is not enough to cause a previously impacted and impermeable specimen to leak. Again, due to the small number of test specimens, further testing needs to be conducted in this area to confirm these results.

As a quick summary, the primary results of this research are as follows:

- Aluminum foil, Aluminized Mylar®, and β-titanium 15-3 hybrid composites were successfully manufactured and found to be leak free.
- All specimens remained leak free after thermal cycling
- All hybrids exhibited an increase in critical impact energy, with the β-titanium 15-3 (resin) hybrid exhibiting in excess of 3.5 times the CIE of the control.

As a whole, this research provides promising results for the future applications of graphite/epoxy hybrid composites. As the material of the LH_2 and LO_2 fuel tanks and feedlines, these materials will be expected to withstand extreme thermal stresses and low-velocity impacts while retaining their impermeability. Results from this research indicate that the addition of a barrier layer, embedded within a graphite/epoxy composite during manufacture, can improve the composites resistance to thermal stresses and resistance to low velocity impacts. In order for these materials to be a viable option for future space applications such as these, more testing needs to be conducted to fully characterize the behavior of these materials. But for the purposes of this project, these hybrid composites are extremely promising candidates to go on for future testing and possible application as the cryogenic fuel tanks and fuel lines of the next generation of reusable launch vehicles.

CHAPTER 7 RECOMMENDATIONS

This section will discuss lessons learned from this research and recommendations for future work. Although this experiment investigated many challenges associated with the use of composite materials for these extreme future space applications, there are many other areas that need to be fully explored before these materials can be safely implemented.

One of the major concerns with this research was the potential variability between composite panels and between the specimens from the same panel. Even within the same panel there was a small range of thicknesses between the specimens. Those closest to the edge of the panel were slightly thinner than those in the middle. Further testing needs to be conducted to determine how this variability in thickness will affect the CIE of the composites. Another concern was that there was a high degree of variability between the CIE of the control panels C1 and C2. The aluminum foil and Mylar® panels all exhibited similar CIEs to one another, which is promising. One way to determine panel and specimen variability in future experiments would be to C-scan the specimens. These images would indicate variability present in the material which could be used to determine if specimens between panels could be compared. It is very important to have consistent material so that the results can be interpreted and applied to future specimens.

Another concern is that the thermal cycling performed for this experiment simulated the cryogenic temperatures of the fuel tanks using LN_2 -196°C (77K), which does not get as cold as the LH_2 -253°C (20K). In order to determine how these hybrid composites will behave when subjected to the more extreme temperatures of the actual cryogenic fuel, further thermal cycling using LH_2 should be conducted. Also, impact

testing should be performed on the composites at cryogenic and elevated temperatures to further characterize the behavior of these hybrid composites.

Another big concern with these hybrid composites is that they may exhibit a reduced interlaminar toughness. The bond between the barrier layer material and the composite is likely the weakest bond of the laminate, so interlaminar toughness tests need to be conducted in order to determine if the addition of the barrier layer causes unacceptable mechanical performance. Additional tests of the mechanical performance of these composites should be conducted. As described previously, by the rule of mixtures, the addition of the barrier layer induces a slight reduction in strength, which needs to be tested experimentally to determine the behavior of these hybrid composites under extreme loads and also fatigue conditions. Exploring various stacking sequences and thicknesses of the barrier layer materials would be beneficial in order to optimize these hybrid composites for minimum permeation and maximum strength.

For future experiments, it would be useful to model and predict the impact damage that would occur in the composites to determine and how the thickness and mechanical properties of the barrier layer would affect this damage. Future work to characterize impact damage rather than simple visual inspection would also be beneficial.

Since polymeric materials tend to embrittle with time, the effect of aging needs to be investigated. Work should also be conducted to investigate the durability of these hybrid composites to determine the effect of multiple cycles on their permeability and mechanical properties.

In order to determine if the impact and thermal cycling results from these coupon specimens can be applied to the behavior of these hybrid composites on an actual structure, more testing should be performed using the exact lay-up and geometry of the

application. Damage resulting from mechanical or thermal stresses depends not only on the material itself, but on many structural properties such as local rigidity and energy absorbed by the support structure.

The results of this research are very promising for the use of these hybrid composites for applications where the structure will be expected to withstand extreme temperatures and low-velocity impacts while remaining impermeable. This research indicates that the addition of a barrier layer can improve a graphite/epoxy's resistance to thermal stresses and low-velocity impacts. While these results provide a good starting point, further investigation on the behavior of these hybrid composites must be conducted to determine if they will be a viable option for use on the LH_2 and LO_2 fuel tanks and feedline of NASA's next generation of RLVs.

REFERENCES

[1] Rogacki, "Row", "The Coming Revolution in Space Transportation," Georgia Institute of Technology Structural Mechanics Seminar Series, Atlanta, GA, February 1, 2001.

[2] Kessler, S. S., T. Matuxzeeski, and H. McManus, "Cryocycling and Mechanical Testing of CFRP for the X-33 Liquid H2 Fuel Tank Structure," ASC 16th Technical Conference Proceedings, Blacksburg, VA, September 9-12, 2001.

[3] Morring, Jr., Frank, "SLI Shifting to Use Kerosene First Stage," *Aviation Week & Space Technology*, April 1, 2002, pp. 28-29.

[4] Wright, R. J., and G. M. Roule, "Large Scale Composite Liquid Oxygen Feedlines for Launch Vehicles," 32nd International SAMPE Technical Conference, Nov 5-9, 2000, pp. 352-359.

[5] Northrup Grumman, "Joint Development for RLV Cryotank Structures: SAMTAV Task #4 Final Review," NASA Langley Research Center, February 23, 2000.

[6] Nguyen, B., "Cryotank Skin/Stringer Bondline Analysis" 44th International SAMPE Symposium and Exhibition, Covina, CA, 1999, pp. 856-868.

[7] National Aeronautics and Space Administration, "Final Report of the X-33 Liquid Hydrogen Tank Test Investigation Team," George C. Marshall Space Flight Center, Huntsville, AL, May 2000.

[8] Nettles, A. T., "Permeability of Composite Materials and Adhesive Bonds of the DC-XA Composite Feedline Program," NASA Technical Memorandum 108483, NASA MSFC, Huntsville, AL, March 1995.

[9] Nettles, A., "Impact Damage Resistance of Carbon/Epoxy Composite Tubes for the DC-XA Liquid Hydrogen Feedline," NASA Technical Paper 3583, September 1995.

[10] Findley, Benjamin C., "Permeability of Impacted Coated Composite Laminates," M.S. Thesis, Georgia Institute of Technology, Atlanta, GA, August 2002.

[11] Freeman, D., and T. Talay, "Reusable Launch Vehicle Technology Program," Acta Astronautica, Vol. 41, No. 11, 1998, pp. 777-790.

[12] Gudaitis, C. N., "High Pressure Cryogenic Composite Tank Qualification," 32nd International SAMPE Technical Conference, Nov 5-9, 2000, pp. 342-351.

[13] Rivers, H. K., J. G. Sikora, and S. N. Sankaran, "Detection of Micro-Leaks through Complex Geometries Under Mechanical Load and at Cryogenic Temperature," 42nd AIAA/ASME/ASCE/AHS/ASC Structures, Structural Dynamics, and Materials Conference and Exhibit, Seattle, WA, April 16-19, 2001.

[14] Whitley, Karen S. and Thomas S. Gates, "Tensile Properties of Polymeric Matrix Composites Subjected to Cryogenic Environments," ASC 16th Technical Conference Proceedings, Blacksburg, VA, Sept. 9-12, 2001.

[15] Schoeppner, G.A., R. Kim, and S.L. Donaldson, "Steady State Cracking of PMCs at Cryogenic Temperatures," 42nd AIAA/ASME/ASCE/AHS/ASC Structures, Structural Dynamics, and Materials Conference and Exhibit, Seattle, WA, April 16-19, 2001.

[16] Kwon, Y.W. and J.M. Berner, "Matrix Damage of Fibrous Composites: Effects of Thermal Residual Stresses and Layer Sequences," Computers & Structures, Vol. 64, No. 1-4, 1997, pp. 375-382.

[17] McManus, H. L., A. Faust, and S. Uebelhart, "Gas Permeability of Thermally Cycled Graphite-Epoxy Composites," ASC 16th Technical Conference Proceedings, Blacksburg, VA, September 9-12, 2001.

[18] Kumazawa, H., T Aoki, T. Ishikawa, and I. Susuki, "Modeling of Propellant Leakage Through Matrix Cracks in Composite Laminates," 42nd AIAA/ASME/ASCE/AHS/ASC Structures, Structural Dynamics, and Materials Conference and Exhibit, Seattle, WA, April 16-19, 2001.

[19] Wang, H., and T. Vu-Kanh, "Low-Velocity Impact Damage in Laminated Composite Materials," Impact Response and Dynamic Failure of Composites and Laminate Materials, Key Engineering Materials, Vols. 141-143, Part 1, 1998, pp. 277-304.

[20] Cantwell, W. J., and J. Morton, "The Impact Resistance of Composite Materials- A Review," Composites, Vol. 22, No. 5, September 1991, pp. 347-362.

[21] Dowling, Norman E., "Mechanical Behavior of Materials – Engineering Methods of Deformation, Fracture, and Fatigue 2nd Ed.", Prentice-Hall Inc., 1999.

[22] Wang, H., and T. Vu-Kanh, "Low-Velocity Impact Damage in Laminated Composite Materials," Impact Response and Dynamic Failure of Composites and Laminate Materials, Key Engineering Materials, Vols. 141-143, Part 1, 1998, pp. 277-304.

[23] Zhong, W. and B. Z. Jang, "Material Design Approaches for Improving Impact Resistance of Composites," Impact Response and Dynamic Failure of Composites and Laminate Materials, Key Engineering Materials, Vols. 141-143, Part 1, 1998, pp. 169-186.

[24] De Freitas, M., A. Silva, L. Reis, "Numerical Evaluation of Failure Mechanisms on Composite Specimens Subjected to Impact Loading," Composites: Part B, Vol. 31, 2000, pp. 199-207.

[25] Choi, H. Y., H.-Y. T. Wu, and F.-K. Chang, "A New Approach to Understanding Damage Mechanisms and Mechanics of Laminated Composites Due to Low-Velocity

Impact: Part I I– Experiments," Journal of Composite Materials, August 1991, pp. 1012-1038.

[26] de Moura, M. F. S. F., and A. T. Marques, "Prediction of Low Velocity Impact Damage in Carbon-Epoxy Laminates," Composites: Part A, Vol. 33, 2000, pp. 361-368.

[27] Finn, S. R. and S. Springer, Composite Plates Impact Damage: an Atlas. Technomic Publishing Co., Lancaster, PA, 1991.

[28] Mahfuz, H., M. Saha, R. Biggs, and S. Jeelani, "Damage Tolerance of Resin Infiltrated Composites Under Low Velocity Impact - Experiment and Numerical Studies," Impact Response and Dynamic Failure of Composites and Laminate Materials, Key Engineering Materials, Vols. 141-143, Part 1, 1998, pp. 209-234.

[29] Hsieh, C. Y., A. Mount, B. Z. Jang, and R. H. Zee. "Response of Polymer Composites to High and Low Velocity Impact," 22nd International SAMPE Technical Conference, Boston, MA, November 6-8, 1990, pp. 14-27.

[30] Kim, J.-K., "Methods for Improving Impact Damage Resistance of CFRPs," Impact Response and Dynamic Failure of Composites and Laminate Materials, Key Engineering Materials, Vols. 141-143, Part 1, 1998, pp. 149-168.

[31] Riess, G. and Y. Jolivet, "Rubber-Modified Polymers. Location of Block Copolymers in Two-Phase Materials," Chapter 22, Copolymers, Polyblends, and Composites. Advances in Chemistry Series, American Chemical Society, Washington D.C., 1975, pp. 243-256.

[32] Findley, B. C. and Johnson, W. S., "Benefits of Surface Coatings for Impacted Composites to be Used for Cryogenic Tankage", AIAA Journal of Spacecrafts and Missiles, (accepted December 2003)

[33] ASTM D1434, "Standard Test Method for Determining the Gas Permeability Characteristics of Plastic Film and Sheeting," American Society for Testing and Materials, West Conshohocken, PA, 1982.

[34] Findley, B. C., and Johnson, W. S., "Benefits of Surface Coatings for Impacted Composites to be Used for Cryogenic Tankage ", Proceedings of the 44th AIAA/ASME SD&M Conference, April 2003.

[35] Grimsley, Brian, Cano, Roberto, Johnston, Norman, Loos, Alfred, McMahon, William, "Hybrid Composites for LH2 Fuel Tank Structure", NASA LaRC, NASA MSFC, 2001

[36] Humpenoder, J., "Gas Permeation of Fiber Reinforced Plastics," Cryogenics, Vol. 38, No. 1, 1998, pp. 143-147.

[37] Evans, Robert E, Masters, John E., and Courter, Jeanne L., "Improved Impact and Delamination Resistance through Interleafing", Key Engineering Materials, v37, 1989

[38] Masters, John E, "Structural Performance and Impact Resistance of Advanced Interleafed Materials", International SAMPE Symposium and Exhibition, v34, n pt2, 1989

[39] Magnamite IM7 (5000) Product Data Sheet, Hexcel Fibers, http://www.hexcelfibers.com, March 2002.

[40] Magnamite IM7 (6000) Product Data Sheet, Hexcel Fibers, http://www.hexcelfibers.com, March 2002.

[41] Sankar, Bhavani and Ifju, Peter, "Fiber Reinforced Composites for Hydrogen Storage Systems", Center for Advanced Composites, University of Florida (2003) http://www.fsec.ucf.edu/hydrogen/pdf-slides-01-2003/sankar-task2.pdf

[42] Cytec Engineered Materials, Technical Data Sheet, Cycom 977-2 Toughened Epoxy Resin, http://www.cytec.com/business/EngineeredMaterials/Cycom%20977-2.htm

[43] Pavlick, Matt and Johnson, W.S., "Characterization of Mechanical Properties of Advanced Polymeric Systems Evaluated For a Cryotank Environment" M.S. Thesis, Georgia Institute of Technology, Atlanta, GA, April 2003.

[44] Schaffer et al, "The Science and Design of Engineering Materials, 2nd edition", WCB McGraw-Hill 1999

[45] MatWeb Material Property Data Sheet, http://www.matweb.com

[46] Alcoa 11xx Material Property Data Sheet, http://www.alcoa.com/alumina/en/home.asp

[47] Key To Metals, "Properties of Aluminum Alloys at Cryogenic and Elevated Temperatures", http://www.key-to-metals.com/printarticle.asp?ID=23